Marine Geology 434 (2021) 106439

Contents lists available at ScienceDirect

Marine Geology

journal homepage: www.elsevier.com/locate/margo

Suspended particulate matter in a submarine canyon (Whittard Canyon, Bay of Biscay, NE Atlantic Ocean): Assessment of commonly used instruments to record turbidity

Sabine Haalboom [a,*], Henko de Stigter [a], Gerard Duineveld [a], Hans van Haren [a], Gert-Jan Reichart [a,b], Furu Mienis [a]

[a] NIOZ Royal Netherlands Institute for Sea Research, Department of Ocean Systems, PO Box 59, 1790 AB Den Burg, Texel, the Netherlands
[b] Utrecht University, Faculty of Geosciences, 3584 CD Utrecht, the Netherlands

ARTICLE INFO

Keywords:
Suspended particulate matter
Nepheloid layers
Whittard Canyon
Optical and acoustic sensors
Turbidity
Particle size distribution

ABSTRACT

Nepheloid layers with elevated concentrations of suspended particulate matter (SPM) are found throughout the world's oceans. They are generated by both natural processes, involving resuspension of seabed sediment by bottom currents, and anthropogenic sediment resuspension due to bottom trawling, dredging and in the future potentially due to deep-sea mining. These nepheloid layers represent pathways of lateral SPM transport, including lithogenic and biogenic sediment, organic matter, (trace) metals, organic pollutants and plastics. For assessment of the dispersion of these materials, it is essential that SPM mass concentrations can be accurately quantified. However, this is not straightforward as the detected turbidity signal, which is used as a proxy for SPM mass concentration, not only depends on the concentration of particles, but also on physical characteristics of these particles, such as particle size, substance and shape. Here we present a comparative study of turbidity data to assess the potential implications different sensors have on the estimates of SPM mass concentration. Optical backscatter sensors (OBSs), transmissometers and both low- and high-frequency ADCPs were deployed simultaneously in the Whittard Canyon (North Atlantic Ocean), and water samples were collected for quantification of SPM mass concentration and ex-situ particle size analysis. We found that SPM mass concentrations inferred from the transmissometer are easily overestimated in the biologically productive surface layer due to higher light absorption by chlorophyll-bearing phytoplankton, compared to suspended detritic particles. Furthermore, we observed that depending on sensor type some particles are not, or less well, detected. This is due to differences in particle size sensitivities of these sensors towards the diverse range of particle sizes found in the Whittard Canyon, whereby the low-frequency ADCP was most sensitive for coarse-grained material and the high-frequency ADCP and OBSs most sensitive for fine-grained material. In future studies, we suggest to use a combination of different sensors as the use of only one type of sensor could potentially lead to misinterpretation and misquantification of particle transport processes and fluxes.

1. Introduction

Throughout the world's oceans, and in particular along continental slopes, suspended particulate matter (SPM) is found in elevated concentrations in so-called nepheloid layers (McCave, 1986; Durrieu de Madron, 1994; Amin and Huthnance, 1999; Gardner et al., 2018a). Generally these nepheloid layers occur in areas where the hydrography interacts with the topography (Gardner et al., 2018b), which is often related to the incidence of internal waves in areas with a (super-)critical slope (Quaresma et al., 2007; Puig et al., 2014; van Haren et al., 2015). These energetic hydrodynamics result in resuspension and dispersal of (food) particles (Dickson and Mccave, 1986; Amin and Huthnance, 1999), thereby influencing deep-sea ecosystems (Mienis et al., 2007; Davison et al., 2019). In a very different setting, nepheloid layers are also observed along mid-ocean ridges and back-arc basins where they can be traced back to hydrothermal vents emitting plumes rich in very fine-grained particulates. These plumes rise several hundred metres above the seafloor and disperse over vast areas, providing a major

* Corresponding author.
E-mail address: sabine.haalboom@nioz.nl (S. Haalboom).

https://doi.org/10.1016/j.margeo.2021.106439
Received 4 August 2020; Received in revised form 30 January 2021; Accepted 3 February 2021
Available online 8 February 2021

source of heat and chemicals to the ocean (German et al., 1998), hereby affecting the local geochemistry and biodiversity (Khripounoff et al., 2001; Haalboom et al., 2020). Anthropogenic disturbances are also recognised as a cause of the formation of nepheloid layers. Bottom trawling (Puig et al., 2012; Daly et al., 2018) and dredging operations (Smith and Friedrichs, 2011) cause resuspension of bottom sediment, often interfering with natural sediment transport processes (Martín et al., 2014). Moreover, in the foreseeable future, anthropogenic nepheloid layers may also make their appearance in hitherto pristine deep-sea environments, as a consequence of the mining of polymetallic nodules and seafloor massive sulphide deposits (Glover and Smith, 2003; van den Eynde et al., 2014).

Submarine canyons, of which almost 6000 have been identified worldwide (Harris and Whiteway, 2011), appear to be hotspots for the generation of nepheloid layers, which makes them ideal locations to study SPM dynamics. Within submarine canyons the formation of these layers is driven by energetic hydrodynamics often associated with intensified internal wave activity, as for example demonstrated in canyons along the Portuguese margin (de Stigter et al., 2007, 2011; Quaresma et al., 2007), US margin (Gardner, 1989) and the Bay of Biscay (Wilson et al., 2015; Hall et al., 2017). In submarine canyons, nepheloid layers are thought to serve as a link between the biologically productive continental shelves and the organic-matter starved deep sea, thereby playing a prominent role in carbon and nitrogen cycling (Gardner, 1989; Durrieu de Madron, 1994; Puig and Palanques, 1998; Amin and Huthnance, 1999; Kiriakoulakis et al., 2011; Canals et al., 2013; Puig et al., 2014). Evidence for enhanced organic matter transport from the continental margins to the deep sea via canyons (Jahnke et al., 1990; Walsh, 1991) is the elevated standing stock of benthic fauna found in submarine canyons compared to their adjacent open slopes (De Leo et al., 2010; Huvenne et al., 2011; Robertson et al., 2020).

Nepheloid layers play a major role in particle transport, including detritic, biogenic sediment, organic matter, (trace) metals, organic pollutants adsorbed to particles and plastics. Therefore, it is important that these particle loads are properly quantified. For example, within submarine canyons quantification of fluxes of organic matter will aid to the understanding of food supply to the deep sea and transport and burial of carbon (Thomsen, 1999; Duineveld et al., 2001; Epping et al., 2002; García and Thomsen, 2008; Amaro et al., 2015), and at hydrothermal vent sites it has been shown that the diversity of microorganisms changes within the chemically enriched hydrothermal plumes as they disperse away from the vent site (Haalboom et al., 2020). In the case of anthropogenic plumes, a proper quantification is also important to assess the extent of plumes, as they can potentially smother benthic fauna (Kutti et al., 2015). This is especially the case in deep-sea settings where sediment plumes do not naturally occur, and life is adapted to extremely low suspended particle concentrations (Boschen et al., 2013).

For the detection of SPM and nepheloid layers, optical sensors (optical backscatter sensors (OBSs) and transmissometers) find widespread application. Acoustic devices, like acoustic Doppler current profilers (ADCPs), which are commonly used for recording current speed and direction, do also record turbidity on the basis of intensity of backscattered acoustic signal. These optical and acoustic sensors, operating at different optical wavelengths and acoustic frequencies, are used to detect relative changes in turbidity in the water column. Quantification of turbidity data in terms of mass concentration of SPM so far remains complex (e.g. Guillén et al., 2000; Downing, 2006; Fettweis et al., 2019), as the detected signal is not only dependent on the concentration of particles, but also on particle size distribution and aggregation (Baker and Lavelle, 1984; Bunt et al., 1999; Hatcher et al., 2001; Gruber et al., 2016; Sahin et al., 2020), shape and surface roughness (Gibbs, 1978; Schaafsma and Hay, 1997), composition (Maa et al., 1992; Moate and Thorne, 2012; Ohnemus et al., 2018) and colour of the material (Hatcher et al., 2000).

To date, mainly laboratory studies have been performed to examine the effects of the physical properties of particles on turbidity measurements (e.g. Baker and Lavelle, 1984; Downing and Beach, 1989; Gibbs and Wolanski, 1992; Hatcher et al., 2000; Sahin et al., 2020) and field studies which have directly addressed the merits and potential drawbacks of commonly used turbidity sensors often only considered one type of sensor (e.g. Bishop, 1986; Merckelbach and Ridderinkhof, 2005; Perkey et al., 2010; Guerrero et al., 2011; Boss et al., 2015; Santos et al., 2020). Inter-comparisons of sensors by e.g. Osborne et al. (1994), Hawley (2004), Lewis et al. (2007), Rymszewicz et al. (2017), Fettweis et al. (2019) and Lin et al. (2020) were performed in onshore (rivers and lakes) and near-shore settings, where very high particle loads, varying contribution of sand-sized particles and formation of aggregates proved challenging for quantification of SPM mass concentrations. Open ocean settings pose different challenges to the quantification of SPM due to the large depth preventing frequent sampling for calibration and because of the large contribution to SPM of both living plankton as well as organic and inorganic detritus. Small-sized primary particles have the tendency to aggregate into larger aggregates that have different optical and acoustic properties. In addition, migrating zooplankton can produce a distinct acoustic backscatter signal in low-frequency ADCPs (Flagg and Smith, 1989; Plueddemann and Pinkel, 1989; van Haren, 2007). Given the past and current studies employing turbidity sensors in open ocean settings, and the many studies to come prompted by increasing human disturbance of the seafloor (e.g. dredging, deep-sea mining), a better understanding of what the different types of turbidity sensors are recording in these settings is needed (Ziegler, 2002; Puig et al., 2014; Rymszewicz et al., 2017). Thereby it is of importance that the output of these sensors can be properly quantified in terms of SPM mass concentration and that processes affecting flocculation and disaggregation are understood, which have possible implications on the quantification of turbidity signals.

In this study, turbidity data, obtained with commonly used commercial optical sensors and acoustic devices, are compared. Sensors were deployed simultaneously in the Whittard Canyon (northern Bay of Biscay, NE Atlantic Ocean), which is known for its ubiquitous presence of nepheloid layers over a wide range of concentrations (Wilson et al., 2015). Furthermore, the presence of biologically productive surface water during spring, allowed for comparison of sensor output for surface water containing primarily live plankton versus bottom water containing a mixture of detritic lithogenic and biogenic sediment particles. The differences in turbidity records produced by simultaneously deployed sensors and the respective implications on estimates of SPM mass concentration are discussed. Moreover, we apply these findings on a time series collected with these sensors to investigate the near-bed SPM dynamics.

2. Regional setting

The Whittard Canyon (Fig. 1) is a dendritic submarine canyon system, incising the Celtic continental margin in the northern Bay of Biscay (Amaro et al., 2016). The four main, NNW-SSE to NNE-SSW oriented branches of the canyon system extend from the continental shelf at approximately 200 m water depth to the abyss at depths exceeding 3500 m, where the branches converge in the so-called Whittard Channel (Amaro et al., 2015).

The hydrodynamic regime within the Whittard Canyon is characterised by semi-diurnal tidal currents, dominated by the principal lunar semi-diurnal (M_2) component (Pingree, 1980; Holt and Thorpe, 1997; Hall et al., 2017). The complex sloping topography together with the across-slope tidal flow results in the generation and reflection of internal waves and tides at the shelf edge and the upper reaches of the canyon (Hall et al., 2017). These enhanced hydrodynamics cause elevated mixing near the seafloor, resuspending sediment and organic matter and facilitating along-canyon transport by means of intermediate nepheloid layers which are formed as lateral extensions of the bottom nepheloid layers (Wilson et al., 2015). In addition gravity flows initiated by trawling at the interfluves in between different branches of the canyon

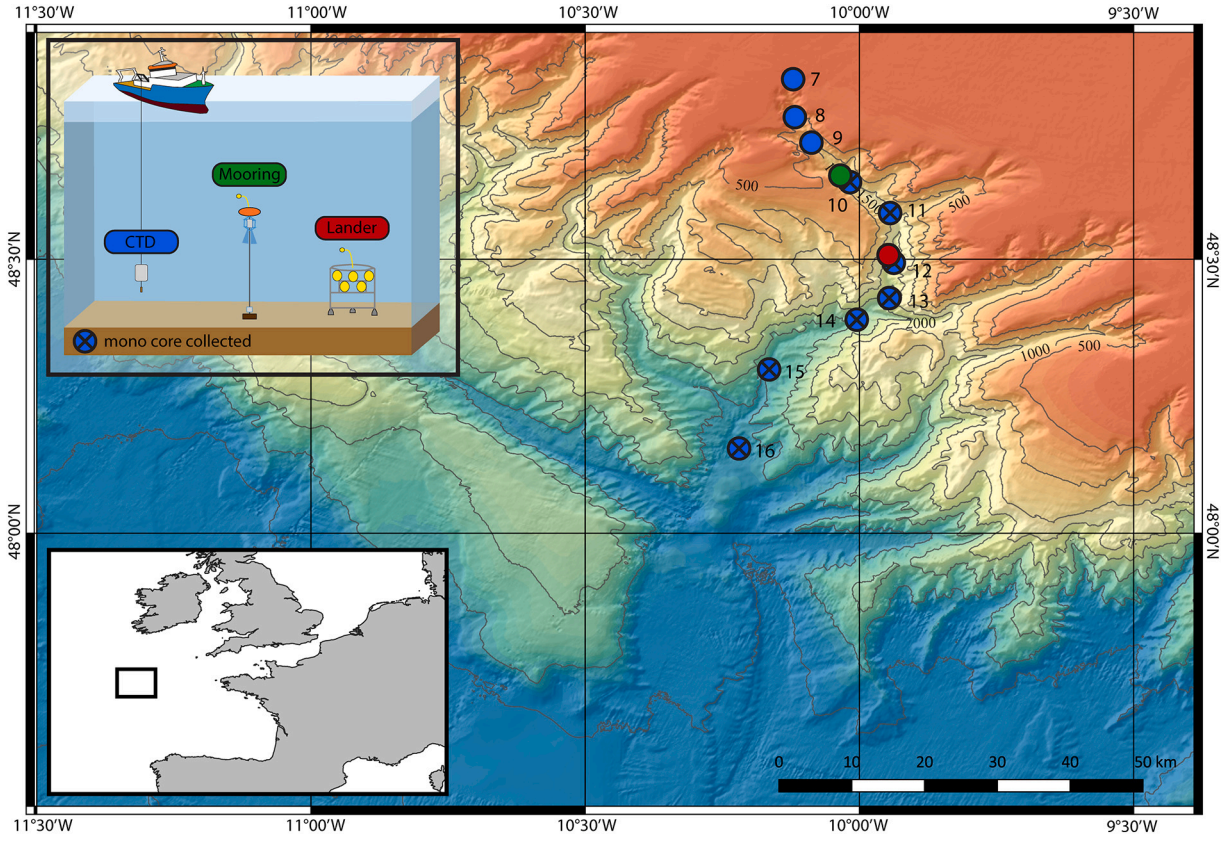

Fig. 1. Geographical location (lower left inset) and bathymetric map of the Whittard Canyon in the Bay of Biscay, NE Atlantic Ocean (bathymetry from EMOD data base), showing the location of CTD stations 7 to 16 and mooring and lander deployments in the easternmost canyon branch, as well as locations where mono cores were collected (marked with x).

result in sediment laden near-bottom plumes with high concentrations of organic material (Daly et al., 2018), a phenomenon observed previously in the Palamós Canyon in the Western Mediterranean (Puig et al., 2012).

3. Material and methods

Sensors discussed in this study were deployed in May 2017 and May 2018 during RV *Pelagia* cruises 64PE421 and 64PE437, in three different configurations (for details see Table S1):

1) Two optical backscatter sensors (WetLabs ECO FLNTU and JFE Advantech Infinity, operating at 700 and 880 nm respectively), next to the standard WetLabs C-Star transmissometer, operating at 650 nm, were mounted on a profiling SeaBird 911 CTD-Rosette system. The CTD-Rosette, which among various other sensors also held a fluorometer, was hauled through the water column, allowing comparison of sensor output in productive surface waters with high fluorescence, in clear mid-waters and in a bottom nepheloid layer loaded with fine particulate matter as shown by particle size analysis (see Section 5.1).
2) A bottom lander was deployed for two days in the canyon axis at 1915 m water depth, equipped with two optical backscatter sensors (WetLabs ECO FLNTU and JFE Advantech Infinity) and a high-frequency (1 MHz) sideways-looking Nortek Aquadopp ADCP at 1 m above bottom (mab) (with 1 m blanking distance). Sampling frequency was set to five minutes (with data recorded at 1 Hz and averaged over 60 measurements) for all sensors, allowing for comparison of sensor output under highly variable bottom water turbidity produced in a regime of oscillating tidal currents.
3) A 430 m long oceanographic mooring was deployed for nine days in the canyon axis at 1400 m water depth, equipped with a JFE Advantech Infinity OBS at 5 mab, a downward-looking low-frequency (75 kHz) RDI Workhorse Long Ranger ADCP at 410 mab (with a blanking distance of 23.28 m and vertical intervals binned over 5 m), and a string of 200 high-precision thermistors (van Haren et al. 2009). Data from the thermistor string will be published elsewhere, except for a time-series record of vertical isotherm fluctuations. Sampling frequency was set to one minute for the turbidity sensors (with data recorded at 9 pings per ensemble (6 s per ping) for the ADCP and one measurement per minute for the JFE Advantech OBS), allowing for a comparison as under 2, but with a different acoustic frequency. In this study only the data from the lowermost bin which is not affected by interference with the seafloor is shown. The validity of this data was tested by calculating the signal-to-noise ratio (SNR) based on the equation given in the Teledyne RDI application note (Mullison, 2017), which resulted in an average SNR of 39, with less than 6% of the data having a SNR < 10. The data for this bin is located 45 m above the seafloor and therefore 40 m above the JFE OBS.

Backscatter and transmission data produced by the optical sensors mounted on the CTD Rosette were correlated to SPM mass concentration (mg L^{-1}). In parallel with the optical measurements, SPM was collected by filtering duplicate 5 L portions of Niskin water samples over 47 mm 0.4 μm pre-weighed Millipore polycarbonate filters (Table S2). The filters were rinsed with Milli-Q to remove salt and stored at −20 °C until further analysis. In the laboratory at NIOZ, the filters were freeze-dried, rinsed once more with Milli-Q to remove any remaining salt, freeze-dried again and then weighed to determine the amount of SPM per volume of filtered seawater. The nature of the collected SPM was

investigated by examining a selection of 12 representative filter samples with a Hitachi TM3000 scanning electron microscope (SEM).

The SPM particle size distribution in surface, intermediate and bottom nepheloid layers as well as in clear water was determined from Niskin water samples collected from various depths in the canyons (Table S2). The samples were left standing in the dark for over a month at 5 °C in order to make sure all SPM settled, following Stokes' Law for particles with a radius of 1 μm or larger. The overlying water was carefully siphoned off and the remaining water with SPM was divided equally over two 40 mL bottles. After adding 5 mL 0.1 M Na-pyrophosphate to prevent flocculation of the material, the subsamples were analysed in duplicate with a Beckman Coulter LS 13320 laser particle sizer, using the micro cell measuring mode, with a minimum of three runs for each sample.

Similarly the particle size distribution of surface sediments (0–0.5 cm) was determined for seven locations along the canyon's axis (Fig. 1, Table S3). Sediment samples were collected using a NIOZ designed mono corer which was suspended 7 m below the CTD-Rosette frame. Collected mono cores were sliced on board in 0.5 cm slices and were subsequently stored at a temperature of −20 °C. Prior to analysis, samples were freeze dried for 3 days to ensure adequate removal of water. For analysis of particle size distribution a subsample was taken and was suspended in reverse osmosis demineralised water. After adding 10 mL Na-pyrophosphate to prevent flocculation of the material, the subsamples were analysed with a Beckman Coulter LS 13320 laser particle sizer, using the large volume cell, with a minimum of three runs for each sample.

4. Theory

Although sensor-specific differences in response to different types of SPM generally hinder a straightforward conversion of measured turbidity to SPM mass concentration, optical and acoustic sensors have in common that they have a physically well-understood relationship between sensor response and concentration and size of the detected particles, within certain limits and for ideal spherical particles.

Optical backscatter sensors such as used and discussed in this paper basically measure relative changes in concentration of particles in a suspension based on changes in intensity of backscattered light. Transmissometers work the opposite, and measure relative changes in concentration of particles on the basis of changes in intensity of transmitted light. Within the specified operational range of the sensor, the backscattered or transmitted light intensity is linearly related to the concentration of suspended particles, provided that the physical parameters of the particles remain constant (Baker and Lavelle, 1984; Downing, 2006; Hill et al., 2011). At higher concentrations, beyond the limit where the sensors get saturated, the increase in backscattered light or decrease in transmitted light with increasing particle concentration flattens off until there is no change in response with increase in particle concentration. With further increase in concentration, backscatter will eventually start to decrease due to the so-called grain shielding effect (Bunt et al., 1999), causing multiple scattering and interference of the backscattered signal (Kineke and Sternberg, 1992; Downing, 2006).

The response of both types of optical sensors is dependent on the particle size distribution of the SPM, complicating the quantification of the detected signal. The response of the OBS is inversely proportional to the size of the particles, as it has been shown that the OBS response is lower for suspensions with coarser particless, than for suspensions of similar mass concentrations with finer grained material (e.g. Gibbs and Wolanski, 1992; Bunt et al., 1999; Hatcher et al., 2001; Downing, 2006). This is explained by the decreased area-to-volume ratio of larger particles and thereby a smaller projected area (Hatcher et al., 2001). The same applies to the transmissometer, of which the response is dependent on the absorption and scattering of particles (c_p) and absorption by water (c_w) (Jerlov, 1976), with c_p being dependent on the total particle cross-sectional area (van de Hulst, 1957). Again, for similar mass concentration of particles, sensor response is stronger for smaller particles than for larger ones.

Acoustic devices such as the ADCPs discussed in this paper, measure relative changes in concentration of particles in a suspension based on changes in intensity of the backscattered acoustic signal, analogous to the principle of optical backscatter. For acoustic devices, however, the sensor response is not linearly related to SPM mass concentration (e.g. Fugate and Friedrichs, 2002). Commonly, the acoustic backscatter is expressed in counts, which is proportional to decibel sound pressure level (SPL). In the study of Merckelbach and Ridderinkhof (2005) the following equation (Eq. 1) is given for SPL, based on the random phase backscatter model presented by Thorne and Hanes (2002):

$$SPL\,[dB] = 10log_{10}\left(K_R\frac{k^4\langle a_s^6\rangle}{\rho_s\langle a_s^3\rangle}SPM\frac{e^{-4r\alpha}}{r^2}\right) \quad (1)$$

In which K_R is the device dependent calibration coefficient, k is the acoustic wave number, a_s is the particle diameter, ρ_s the density of the scattering particles, SPM the SPM mass concentration, r the distance from transducer to bin and α the coefficient of attenuation. The acoustic wave number k is defined as:

$$k = \frac{2\pi f}{c} \quad (2)$$

In which f is the frequency of the acoustic wave and c the speed of sound. From Eq. 1 it follows, with physical characteristics of the particles and water remaining constant, that the SPL at any distance within the measuring range is logarithmically proportional to the SPM mass concentration ($SPL \propto 10log_{10}(SPM)$).

The acoustic backscatter response of ADCPs to differently sized particles is dependent on the operating frequency of the ADCP (Wilson and Hay, 2015). This is expressed in different particle size sensitivities for different acoustic frequencies. Peak sensitivity occurs at $k * a = 1$, in which k is the acoustic wave number as defined by Eq. 2 and a is the particle radius, and the detection limit is at $k * a = 0.05$, as long as there is no significant concentration of particles with $k * a \approx 1$ (Lohrmann, 2001). Given the mean speed of sound (c) in seawater of 1525 m s^{-1}, a 75 kHz ADCP such as used in the mooring in this study has a peak sensitivity for particles with a diameter of 6475 μm and a lower detection limit for particles with diameter of 323 μm. For the 1 MHz ADCP, such as mounted on the bottom lander, peak sensitivity and lower detection limits are for particle diameters of, respectively, 485 μm and 24 μm. From the above it follows that the 1 MHz ADCP has its peak sensitivity at a particle size for which the 75 kHz ADCP is close to its lower detection limit.

5. Results and discussion

5.1. Optical backscatter and light transmission in surface, intermediate and bottom nepheloid layers

A CTD transect along the axis of the easternmost Whittard Canyon branch, covering a depth range of 185 to 3644 m water depth (Fig. 1), showed the ubiquitous presence of intermediate and near-bottom nepheloid layers at canyon depths between 900 and 2800 m water depth, with highest turbidity signals found between 1250 and 1750 m water depth (Fig. 2). All three sensors mounted on the CTD, the WetLabs FLNTU and JFE Advantech OBSs and the WetLabs C-Star transmissometer, showed relatively low turbidity at intermediate water depths and increasing values towards the bottom nepheloid layer. The presence of nepheloid layers in the Whittard Canyon is a permanent feature, as it was also observed during previous surveys by Wilson et al. (2015). In comparison with the two types of OBSs that recorded only modestly elevated turbidity at the surface, the transmissometer also measured distinctly higher turbidity in the surface layer (Fig. 2). The deviating sensor response in the surface layer of the transmissometer

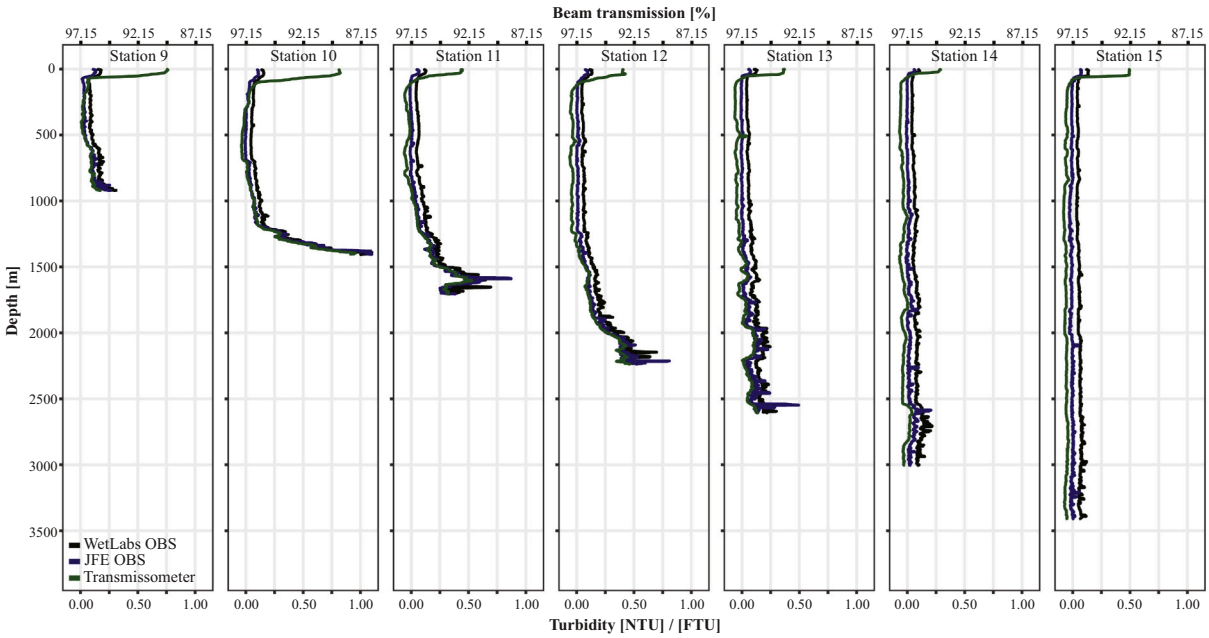

Fig. 2. CTD profiles showing the turbidity measured by the WetLabs FLNTU OBS (black), JFE Advantech OBS (blue) and WetLabs C-Star transmissometer (green) of station 9 to 15, recorded down to 7 mab. (For interpretation of the references to colour in this figure legend, the reader is referred to the web version of this article.)

compared to the OBSs is clearly demonstrated in Fig. 3A, where the sensor response of the WetLabs transmissometer is plotted against the response of the WetLabs OBS of all CTD casts. Based on this result and the fact that SPM likely has different characteristics over the water column, two regression lines were calculated for the relationships between sensor output of the WetLabs OBS and WetLabs Transmissometer and the weighed SPM mass concentrations (mg L^{-1}), one for surface samples (<100 m) and one for samples in the lower part of the water column, as shown in Fig. 3B and C respectively. The relationships between the JFE Advantech OBS and the response of the transmissometer and the weighed SPM mass concentration are not shown because of their similarity to the WetLabs OBS. Linear relationships appeared to be an appropriate model for the data with R^2's ranging from 0.70 to 0.95. The relationship between the output of the OBSs does not change significantly when surface and deeper water data are considered separately (ANCOVA, $P = 0.1923$). However, the regression lines clearly illustrate the diverging output of the transmissometer in the surface water (ANCOVA, $P < 0.001$). The slopes of regression lines belonging to the shallow and deep waters are almost the same for the OBS, while they are different in the case of the transmissometer.

The different response of especially the transmissometer to SPM in the surface water and deeper water, as compared to the response of the OBSs, can be explained by the greater sensitivity of the transmissometer to differences in physical properties of the SPM in the surface water and near-bottom water. In the biologically productive surface water, particulate matter detected by the sensors is likely largely composed of living phytoplankton and small zooplankton, as shown by increased fluorescence values in the upper 100 m recorded by the CTD. SPM in bottom nepheloid layer is mostly composed of detritic mineral material and biogenic carbonate and silica. SEM analysis revealed that particulate matter filtered from surface water typically consisted of intact pelagic diatoms, coccolithophores, silicoflagellates and amorphous blots, likely representing organic aggregates. The near-bottom samples were characterised by a mixture of biogenic carbonate, silica and lithogenic material. The stronger response of the transmissometer in the organic-rich surface water may therefore be attributed to a stronger absorption of the emitted light with a wavelength of 650 nm by chlorophyll-bearing phytoplankton (Schoellhamer, 1993; Bunt et al., 1999), compared to the 700 and 880 nm light emitted by the OBSs. This is confirmed by the study of Bricaud et al. (1998), who showed that the absorption coefficient for chlorophyll-bearing material generally increases with decreasing wavelengths.

Although the difference in slopes of the regression lines of the OBS belonging to the shallow and deep water was not significant, the lower response of the OBSs in the surface water could be attributed to the larger average particles sizes (e.g. Gibbs and Wolanski, 1992; Bunt et al., 1999; Hatcher et al., 2001; Downing, 2006), since the particle size of the SPM varied between distinct depths in the water column (Fig. 4). The SPM in the surface water had the largest particle size (median of 43 μm), followed by material in the bottom nepheloid layer (median of 34 μm). The SPM found in the clear midwater had the smallest particle size (median of 18 μm). It should be mentioned that these are the particle size distributions for single particles, as aggregates were broken up during sample preparation for particle size analysis. Therefore, to properly quantify the response of optical turbidity sensors, these differences should be accounted for. If only one uniform regression line is calculated in the case of the transmissometer, SPM mass concentration in the surface layer would be overestimated and SPM mass concentration in the lower part of the water column would be underestimated.

5.2. *Dynamics of SPM in the bottom boundary layer observed with OBSs and 1 MHz ADCP acoustic backscatter*

Lander and mooring deployments, primarily intended for investigating the relationship between current dynamics and suspended sediment transport in the canyon axis, offered an opportunity for comparison of temporal variations in turbidity records obtained by both optical and acoustic sensors. During the two-day deployment of a bottom lander at 1915 m water depth, optical backscatter recorded by the WetLabs and JFE Advantech OBSs and acoustic backscatter recorded by the 1 MHz Nortek ADCP were compared. The near-bottom current regime presented in Fig. 5 shows a distinct semi-diurnal variation in current speed and direction, with a main flow direction alternating between 15° (up-canyon) and 130° (down-canyon) (Fig. 5A), and current speeds ranging from 2 to 20 cm s^{-1}. The OBSs and the 1 MHz ADCP show remarkably comparable patterns in optical and acoustic backscatter (Fig. 5C-E), which is especially evident when the time series are normalised and superimposed (Fig. 5F). The good agreement between the

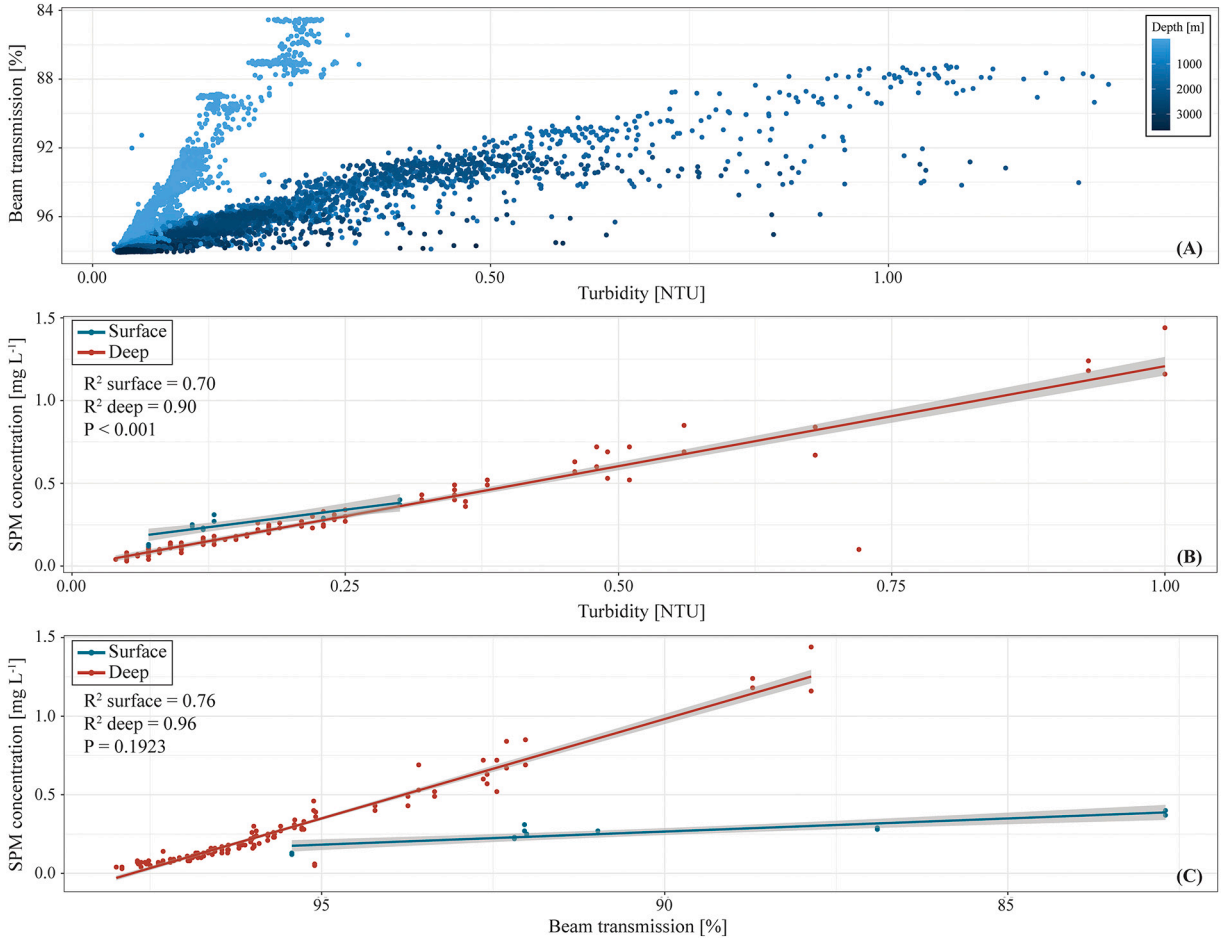

Fig. 3. A) Relation between sensor responses of the WetLabs FLNTU OBS and the WetLabs C-Star transmissometer of CTD stations 7 to 16, colour-coded by depth. B & C) Relation between the recorded turbidity and weighed SPM mass concentrations of the WetLabs FLNTU OBS and WetLabs C-Star transmissometer respectively, with a 95% confidence interval. Blue lines indicate surface samples collected from the upper 100 m of the water column, red lines indicate samples taken at depths greater than 100 m. Statistical analysis was performed in R (R Core Team, 2020) and *P*-values are based on an Analysis of Covariance (ANCOVA) test. (For interpretation of the references to colour in this figure legend, the reader is referred to the web version of this article.)

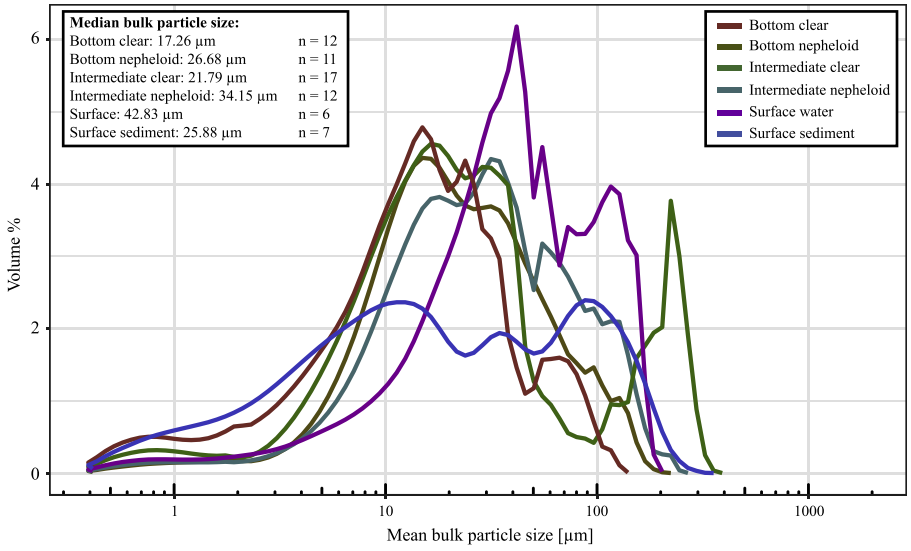

Fig. 4. Average particle size distribution of suspended particulate matter. "Bottom" samples are taken within 10 m from the seafloor, "Surface" samples represent samples collected from the upper 100 m of the water column and "Intermediate" samples are collected between the surface water and the bottom (nepheloid) layer. "Nepheloid" samples are collected from water with a turbidity distinctively higher (>0.1 FTU) than the background turbidity (<0.1 FTU), which is represented here as "Clear". "Surface sediment" samples refer to the 0–0.5 cm slice of the collected mono cores. (For interpretation of the references to colour in this figure legend, the reader is referred to the web version of this article.)

optical and 1 MHz acoustic backscatter is also clearly shown in Fig. 6A. It demonstrates a logarithmic relationship between the sensor outputs (R^2 = 0.83), showing that the suspended particles present in the bottom water of the canyon fell within the sensitivity range of both the OBS and the 1 MHz ADCP. Particle size analysis of near-bottom water samples along the canyon's axis revealed that the median particle size is fining

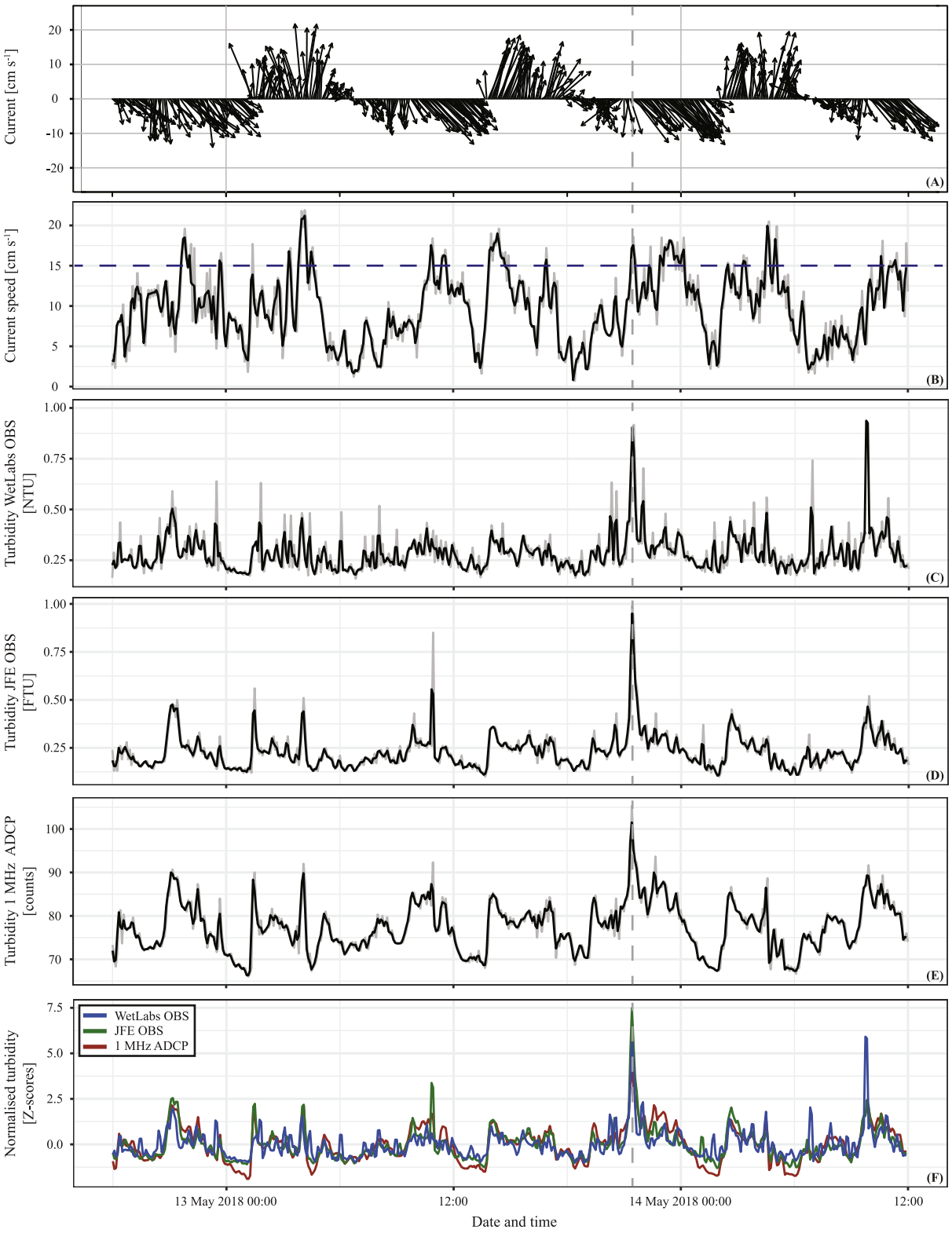

Fig. 5. Near-bottom (1 mab) time series from the lander deployment at 1915 m water depth showing A) current vectors, B) current speed, with blue dashed line indicating the 15 cm s^{-1} threshold for which resuspension of bottom sediment is expected (Thomsen and Gust, 2000), C) turbidity recorded by the WetLabs OBS, D) turbidity recorded by the JFE Advantech OBS, E) turbidity recorded by the 1 MHz Nortek ADCP and F) normalised (Z-scores) turbidity records of the WetLabs and JFE Advantech OBSs and the Nortek 1 MHz ADCP. Normalisation is needed to allow comparing the different turbidity records by converting them to Z-scores, $Z = \frac{x-\bar{x}}{\sigma}$ in which x is the data point, $\bar{x}$ is the average over the complete record and σ the standard deviation. Vertical dashed line marks the interval where the conspicuous turbidity peak is noted in all sensors. (For interpretation of the references to colour in this figure legend, the reader is referred to the web version of this article.)

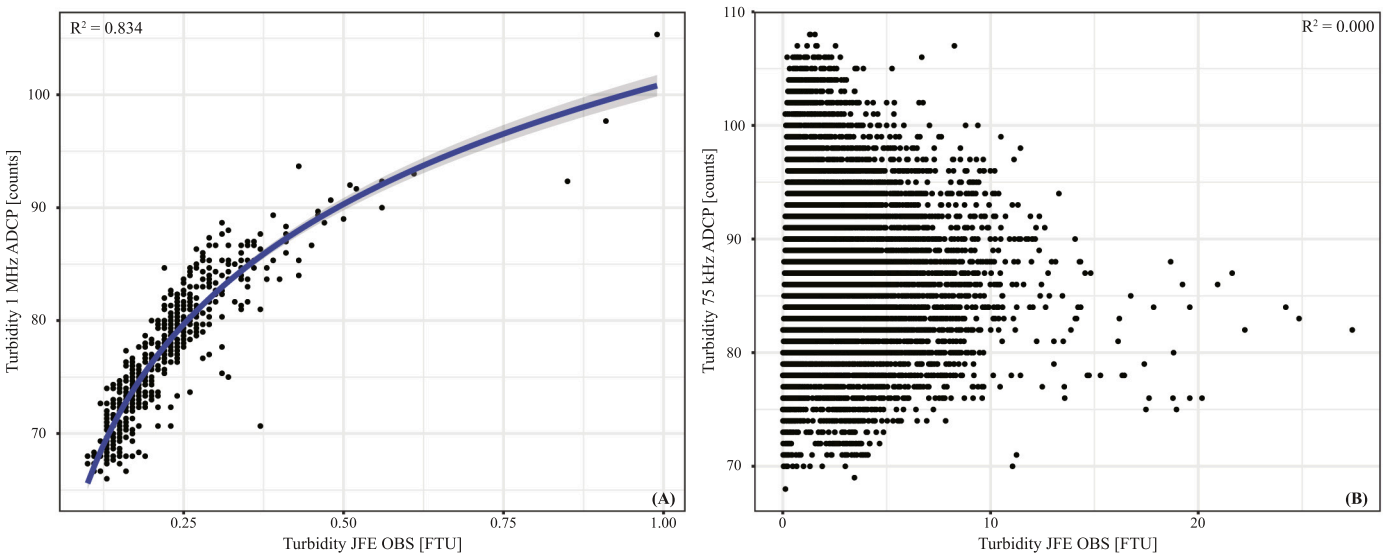

Fig. 6. Relation between recorded turbidity by the JFE Advantech OBS (x-axis) and the ADCPs (y-axis). A) Relation between JFE OBS and the Nortek 1 MHz ADCP; B) Relation between JFE OBS and the RDI Workhorse 75 kHz ADCP.

with increasing distance from the canyon head (Fig. S1). In general the majority of the particles found in the bottom nepheloid layer varied from 8 to 60 μm (D_{10} and D_{90}, respectively) in size (Fig. 4), and at the depth where the lander was deployed a median particle size of 20 μm was determined (Fig. S1). This implies that about half of the suspended particle volume falls below the minimum particle size detection limit (24 μm) of the 1 MHz ADCP. However, it is likely that fine-grained SPM, which in the lab is measured in a fully dispersed suspension, sticks together under natural conditions forming larger-sized organic-mineral aggregates. In such an aggregated form, a larger part of the SPM will fall in the detection range of the 1 MHz ADCP.

The records of both optical and acoustic backscatter from the lander deployment generally show higher values during intervals of higher current speed (Fig. 5F). Minimum values occur systematically with the waning of the down-canyon currents and are followed by an abrupt increase in backscatter as the (tidal) flow reverses from down-canyon to up-canyon direction. This associates with the upslope moving tidal bores that have been observed to resuspend matter on more open bottom slopes (Hosegood et al., 2004). Short-lived peaks in both optical and acoustic backscatter occur mostly, but not exclusively, during intervals of down-canyon flow when current speeds exceed 15 cm s^{-1}. A particularly conspicuous increase in turbidity, recorded by all three sensors, occurred on 13 May between 21:19 and 21:37 h, indicated by the grey dashed lines in Fig. 5. Within this 18-min interval, optical backscatter increased by a factor 2–3, and then decreased again to amounts as measured before. The increase in turbidity coincided with a distinct peak in current speed during an interval of variable current direction, suggesting that the peak in turbidity represents resuspension of sediment from the seabed by local turbulence. During the event the current speed recorded was above 15 cm s^{-1} which is the threshold for sediment resuspension for deep-sea sediment on the Western European margin given by Thomsen and Gust (2000). At this site, sediment on the canyon floor was found to have a similar median particle size as the SPM in the near-bottom water (Fig. S1). The drop in turbidity at the end of the event seems to occur too fast to be simply explained by settling, given the prevalence of fine-grained SPM at this depth in the canyon. If sediment was only locally stirred up, it is conceivable that the turbid plume was quickly swept off by the down-canyon flow. Alternatively, as discussed in more detail in the next section, the sharp peaks in optical backscatter might reflect break-up of larger aggregates into dispersed smaller particles due to increased shear stresses, followed by re-aggregation, as described by Thomsen and Van Weering (1998).

5.3. *Bottom boundary layer SPM dynamics observed with OBS and 75 kHz ADCP acoustic backscatter*

During the nine-day deployment of the mooring at 1400 m water depth, of which a two-day near-bottom excerpt is presented in Fig. 7, a similar semi-diurnal tidal variation in current speed was recorded, with the local main flow direction alternating between 335° (up-canyon) and 155° (down-canyon) (Fig. 7A). Current speed was distinctly higher than at 1915 m where the lander was deployed and ranged from 0 to 40 cm s^{-1}, with peak current speeds up to 70 cm s^{-1}. It should be noted that the current speeds reported here were recorded at 45 mab, which was the depth of the lowermost bin containing valid data, whereas the lander was recording at 1 mab. At this greater height above the seafloor current speeds are likely higher due to a smaller influence of friction with the seafloor. Similar to what was observed during the lander deployment, intervals with higher turbidity in both optical and acoustic backscatter records appear to correspond with intervals of increased current speed (Fig. 7B-D). However, the records of optical backscatter, produced by the JFE Advantech OBS and acoustic backscatter from the RDI Workhorse 75 kHz ADCP do not even remotely match, but display distinctly different patterns (Fig. 7C–E). This could be due to the fact that the OBS and ADCP data were recorded at different heights of, 5 and 45 m above the seabed, respectively. However, the well-developed and more than 100 m thick bottom nepheloid layer observed at this site (Fig. 2, station 10) indicated intense turbulent mixing of the bottom water, allowing comparison, with due caution, of the sensor records. The optical backscatter seemed to respond closely to tidally dominated variations in up- and down-canyon current speed with peaks in backscatter, some representing a five-fold increase in turbidity, coinciding with maxima in current speed. The acoustic backscatter recorded by the 75 kHz ADCP on the other hand displays a broad, irregular saw tooth pattern, repeating itself every cycle of down- to up-canyon flow. Minimum backscatter systematically occurred during the intervals of low current speed when the bottom water flow is turning from up- to down-canyon. From there, acoustic backscatter gradually increased during the interval of down-canyon flow and continued to increase during the subsequent interval of up-canyon flow, to reach a maximum shortly before the up-canyon current was at its maximum strength. When the up-canyon current started to wane, the acoustic backscatter signal steeply dropped to minimum values. Interestingly, and most obvious when the optical and acoustic backscatter records are superimposed (Fig. 7F), the peaks in optical backscatter often did not coincide but rather followed just after

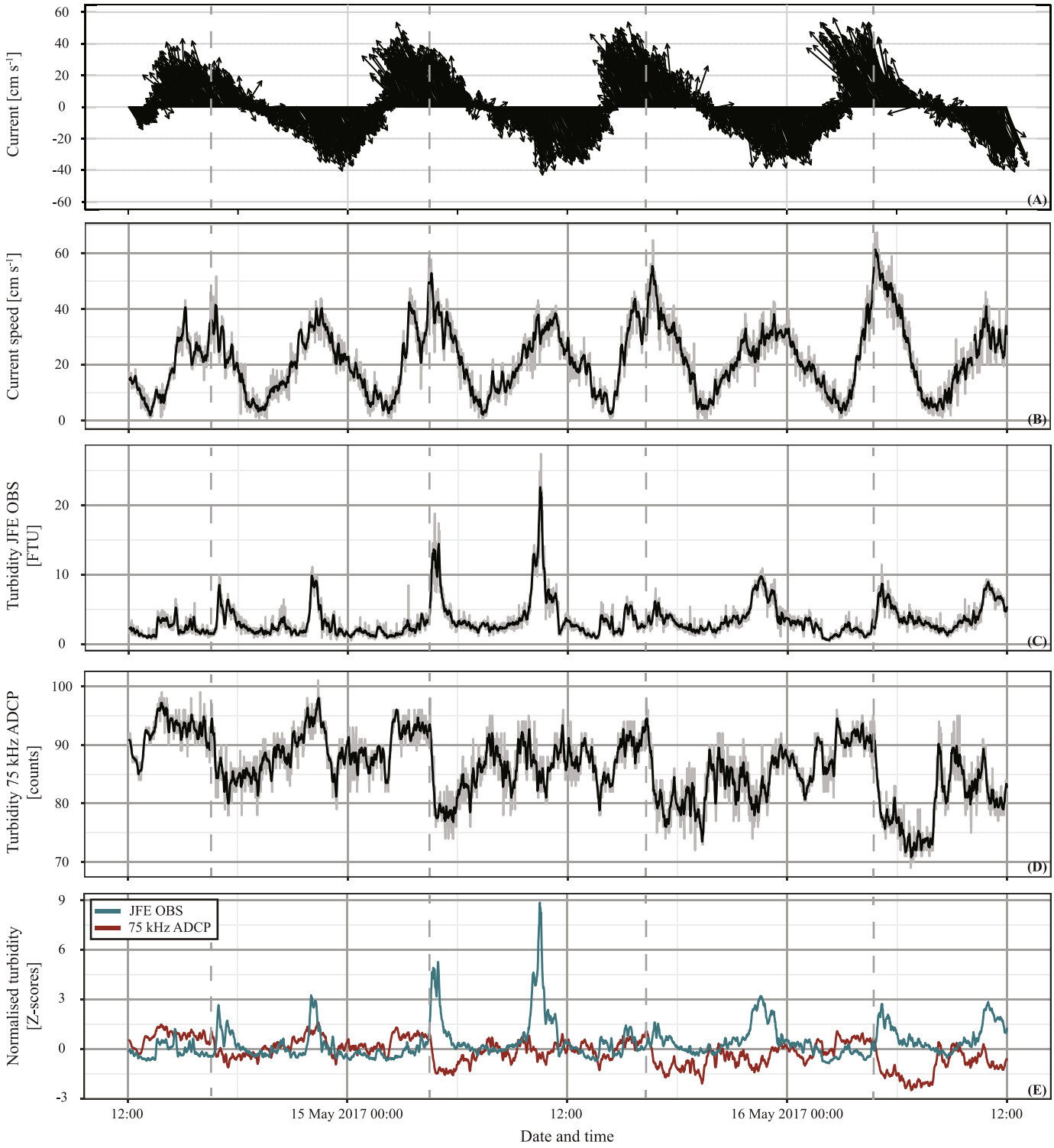

Fig. 7. Two-day part of a near-bottom (45 mab for 75 kHz ADCP and 5 mab for JFE OBS) time series from the mooring deployment at 1400 m water depth showing A) current vectors, B) current speed, C) turbidity recorded by the JFE Advantech OBS, D) turbidity recorded by the RDI Workhorse 75 kHz ADCP and E) normalised (Z-scores) turbidity records of the JFE Advantech OBS and the RDI Workhorse 75 kHz ADCP. Dashed grid lines indicate the time at which the ADCP signal dropped during up-canyon flow. (For interpretation of the references to colour in this figure legend, the reader is referred to the web version of this article.)

peaks in acoustic backscatter, where the latter was already plunging down.

The mismatch between optical and acoustic backscatter, which is also illustrated in Fig. 6B, is comprehended when taking into account that the optical and acoustic sensors have very different sensitivities regarding particle size. Where the optical backscatter sensor is most sensitive for small particles, the 75 kHz ADCP in contrast has its peak sensitivity for relatively large, millimetre-sized particles, whilst it fails to detect particles smaller than a few hundred micrometre. As shown in Fig. S1, the median particle size of SPM collected from the bottom nepheloid layer at the depth where the mooring was deployed, as well as of the surface sediment collected at that depth from the canyon thalweg,

was about 30 μm, well below the lower detection limit of 323 μm given for the 75 kHz ADCP. The larger particles apparent in the acoustic backscatter signal of the ADCP are certainly not massive mm-sized sediment particles (i.e. fine gravel), as such gravel is scarcely present at this depth in the canyon (Fig. 4) and would require far higher current speeds than measured at this site to be resuspended (Thomsen and Gust, 2000; Duineveld et al., 2001).

One possible explanation for the presence of larger particles that produced the backscatter response in the 75 kHz ADCP is that they represent zooplankton or nekton in the mm- or larger size range. Indeed, commercial and scientific devices for detection of fish and zooplankton typically operate in the 50–200 kHz frequency range overlapping with the frequency of our low-frequency ADCP, and there is ample literature on zooplankton/nekton migration based on backscatter data from ship-based or moored low-frequency ADCPs (e.g. Flagg and Smith, 1989; Plueddemann and Pinkel, 1989; Foote, 2001; van Haren, 2007; De Leo et al., 2018; Yang et al., 2019). Moreover, the conspicuous parabolic patterns seen in the time series profile of echo amplitude (Fig. 8), representing the regular vertical oscillation of zones of enhanced backscatter of the ADCP, are reminiscent of acoustic backscatter patterns associated with diel zooplankton migration described by e.g. van Haren and Compton (2013). However, whilst published cases of zooplankton migration typically refer to active diel migration in the upper few tens to hundreds of meters of the water column in response to the day-night cycle, the acoustic backscatter patterns observed in the Whittard Canyon (Fig. 8) are closely following vertical water mass motions marked by the oscillating pattern of isotherms recorded with the thermistor string. These vertical water mass motions, with apparent semi-diurnal frequency and with amplitude of over 200 m at the start of the recorded interval but diminishing towards the end of it, are likely associated with upslope moving internal tidal waves as described by Hosegood et al. (2004) and Hall et al. (2017). The zooplankton/nekton in the aphotic zone (1000–1400 m) of the Whittard Canyon, if indeed that is what was producing the observed backscatter patterns, therefore seems not to be actively migrating but passively following the internal tidal motions, as was also inferred in studies by Ibáñez-Tejero et al. (2018) and Burd and Thomson (2019). Unfortunately, in our present data set from the Whittard Canyon we have no direct observational evidence, from either an underwater camera or plankton net hauls, to verify the nature of the particles producing the low-frequency acoustic backscatter signal. In a number of studies where the relation between recorded ADCP backscatter and in-situ measured zooplankton biomass was verified with plankton net hauls (e.g. Ibáñez-Tejero et al., 2018; Fielding et al., 2004; Briseño-Avena et al., 2018) it was found that zooplankton biomass generally explained only 50% or less of the variability in acoustic backscatter. Based on the physical principles of acoustic backscatter, this might be explained by temporal variation in size distribution of the zooplankton/nekton. However, it should also be considered that at least part of the backscattering particles may be non-living, large aggregates settling out as marine snow through the water column or resuspended from the seabed, possibly in combination with acoustic backscatter of turbulence deformed density stratification.

The importance of particle aggregation and disaggregation processes in fine-grained cohesive sediment dynamics is well-established in the literature (e.g. McAnally and Mehta, 2002), and has been demonstrated both in laboratory studies (e.g. Verney et al., 2011) and in the field (e.g. Markussen and Andersen, 2014). Whilst individual particles in fine-grained cohesive sediment typically are in the size range of a few

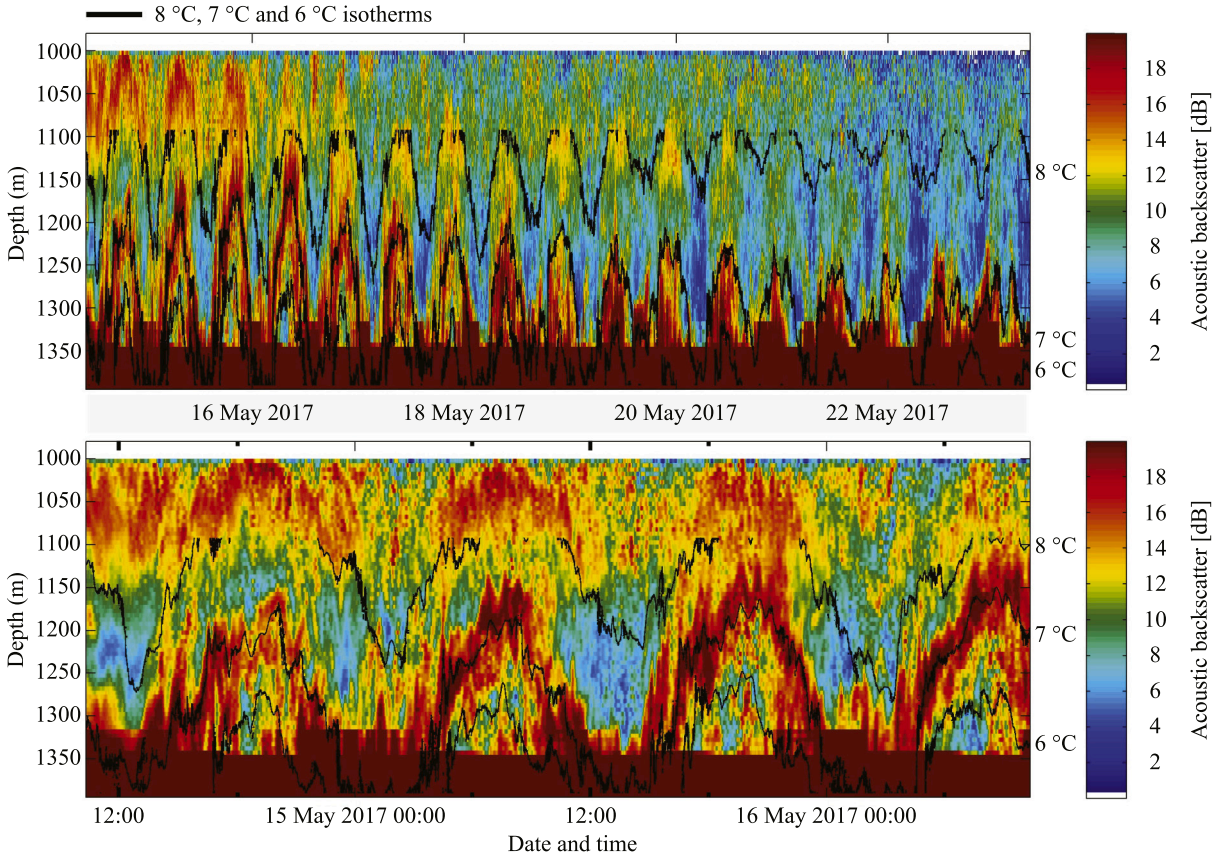

Fig. 8. Time series profile of acoustic backscatter as recorded by the low-frequency (75 kHz) ADCP mounted on the mooring. Echo amplitude counts have been recalculated to dB using the formulas given by Gostiaux and van Haren (2010). Lower end of the profile represents the seafloor. ADCP data shown in Figs. 7 and 9 is recorded at 1350 m (45 mab). The JFE OBS was recording at 5 mab. The black contours represent, from top to bottom, the 8 °C, 7 °C and 6 °C isotherms as inferred from data recorded by the thermistors. Upper figure shows the entire nine-day time series. Lower figure represents the first two days of the time series.

micrometres, with very slow settling velocities in the order of 0.01 mm s^{-1}, aggregation of these particles may produce large aggregates of up to centimetres in size, with settling velocities orders of magnitude higher than of the individual particles of which the aggregates are made up (e.g. van Leussen, 1988; Manning and Dyer, 1999). In the context of the present study, the relevance of the aggregation process is that particle suspensions made up of dispersed individual particles may only be detectable with optical sensors and high-frequency acoustic sensors, whereas in aggregated state they may also become in the detection range for low-frequency acoustic sensors. According to theory, particle concentration and turbulence are important factors in determining aggregation rate and the size to which aggregates may grow. Sufficient particle concentration and moderate turbulence are required to promote particle-particle encounters that lead to aggregation. However, under increasing turbulent shear, fragmentation of aggregates becomes prevalent over formation, leading to a decrease in aggregate size.

In resuspension experiments with natural deep-sea sediments, Thomsen and Gust (2000) and Thomsen et al. (2002) demonstrated that with increasing current speed, organic-mineral aggregates, forming a fluffy layer on top of more cohesive sediment, were the first to be resuspended when a critical shear velocity was surpassed. When the current speed was further increased, shear forces at some point led to the break-up of the relatively large organic-mineral aggregates into smaller aggregates and more finely dispersed particles. When current speed was reduced again, the dispersed particles were observed to re-aggregate into larger and relatively fast-sinking flocs (Thomsen and van Weering, 1998). In the Whittard Canyon, and in submarine canyons in general, conditions are favourable for dynamic aggregation processes. Especially in the upper canyon reaches, suspended particle concentrations are relatively high due to the focusing effect of the canyon topography, and due to frequent resuspension of fine-grained material by topographically enhanced tidal currents. These tidal currents are also responsible for a regime of fluctuating turbulent shear, not only at the seafloor but especially also internally, inducing aggregation at low shear and aggregate break-up at high shear. Unpublished underwater time-lapse video imagery collected in spring 2007 at 2076 m water depth in an adjacent branch of the Whittard Canyon confirms the often aggregated nature of particulate matter in the bottom nepheloid layer. On that occasion, but also for the observations of the present study, which were made in approximately the same time of the year, fallout of phytodetritus following the spring bloom may have contributed to stickiness of particulate matter at the bottom of the canyon, favouring aggregation. Applied to the observations in this study, and as an alternative or complementary to the hypothesis of zooplankton/nekton migrations, the variable acoustic backscatter signal recorded by the 75 kHz ADCP could be interpreted in terms of dynamic aggregation and disaggregation of non-living suspended particulate matter. In this interpretation, the build-up of acoustic backscatter observed during each cycle of down- and up-canyon flow could reflect increasing amounts of large aggregates that were picked up by the current from the canyon floor and entrained in the bottom water flow. The sharp drops in acoustic backscatter that seemed to coincide or even precede the moment that down- and up-canyon current speed reached its maximum could then reflect the fragmentation of larger aggregates. The recurrent peaks in optical backscatter at maximum down- and up-canyon current speed could reflect the moment when more cohesive sediment underlying the fluffy surface layer was also resuspended. However, the fact that optical backscatter on several occasions seemed to peak immediately after acoustic backscatter and already started to decline, may suggest a more direct, causal link between the two signals. In this interpretation, the break-up of larger aggregates at maximum current speed, reflected by a drop in acoustic backscatter, would produce bursts of dispersed finer-grained particles, observed as a sharp increase in optical backscatter. The subsequent steep decrease in optical backscatter and continuing decrease in acoustic backscatter potentially indicates re-aggregation of particles and settling at the waning of the tidal current. Following this hypothesis, the observed vertical pattern in acoustic backscatter (Fig. 8) can be explained by resuspension of aggregated particulate matter by internal tidal waves. The upslope moving tidal bores are the driving mechanism behind the resuspension of material (Hosegood et al., 2004), which is then vertically displaced by the internal waves and settles down when the currents starts to wane.

After the first two-day time interval on which the discussion above was focused (Fig. 7), a marked decrease in overall current speed was noted, and in the last two days peaks in current velocity reached only 20 cm s^{-1} or less (Fig. 9A). This trend of decreasing current speed, also reflected in the 12.5 h average of the current speed, is likely associated with the spring-neap tidal cycle (Hall et al., 2017). Turbidity recorded by the OBS followed the trend of decreasing current speed and especially in the last two days showed a marked decrease (Fig. 9B). This pattern is consistent with the observation that optical backscatter peaked during intervals of increased current speed, reflecting enhanced concentrations of fine-grained SPM, resulting from sediment resuspension and break-up of larger aggregates. Acoustic backscatter recorded by the 75 kHz ADCP displayed an opposite trend to optical backscatter with decreasing current speed, showing an irregular, but consistent, increase towards the end of the nine-day record (Fig. 9C). This is consistent with the interpretation that the acoustic signal is produced by organic-mineral aggregates, large enough to be detected by the 75 kHz ADCP, which increase in abundance and size in a regime of moderate currents, (Thomsen et al., 2002; Fettweis et al., 2006). The observed shorter vertical displacement of both the isotherms as well as the maxima in acoustic backscatter (Fig. 8), can also be attributed to the spring-neap tidal cycle. Turbulence induced by breaking of internal waves remained closer to the seafloor which resulted in less vertical displacement of resuspended material. In addition to that, settling out of aggregates from higher water layers may have increased their abundance near the bottom of the canyon. Similar as already noted for the alternative hypothesis, that the 75 kHz acoustic backscatter signal is reflecting zooplankton/nekton, additional observations that could help to verify the aggregate hypothesis are lacking. The contribution of the different particle sources does deserve to be studied more extensively in future studies, perhaps using particle cameras by which the type of particles can be determined.

5.4. *Implications for quantification and interpretation of SPM dynamics and recommendations for future studies*

The three cases discussed above illustrate how quantification of SPM mass concentration in sea water by means of optical and acoustic sensors may be inherently biased by the choice of sensor in relation to the characteristics of the SPM. Irrespective what type of sensor is used, and within the sensitivity range specific for that sensor, the sensor output will always depend on the concentration of particles, but also on their size and composition. The only truly reliable method for obtaining unbiased SPM mass concentrations seems to be by direct weighing of SPM filtered from representative volumes of water. However, the resolution in space and time of the filtration method is far below what can be achieved with optical and acoustic devices. It is therefore good practice in oceanographic studies to combine the two methods, and use SPM mass concentration determined via filtration of discrete water samples for calibration of simultaneously collected optical and acoustic sensor data.

In the case of CTD water column turbidity profiling, a significant correlation was found between the output of the two types of OBSs and the SPM mass concentrations (Fig. 3B), despite the fact that the data represented SPM from surface water, mid water and bottom water collected at random moments through the tidal cycle. The SPM in the Whittard Canyon thus appeared to be fairly uniform in its backscattering characteristics through time and space. Water column turbidity profiles obtained by the transmissometer turned out to be biased by stronger absorption of transmitted light by chlorophyll-bearing phytoplankton in

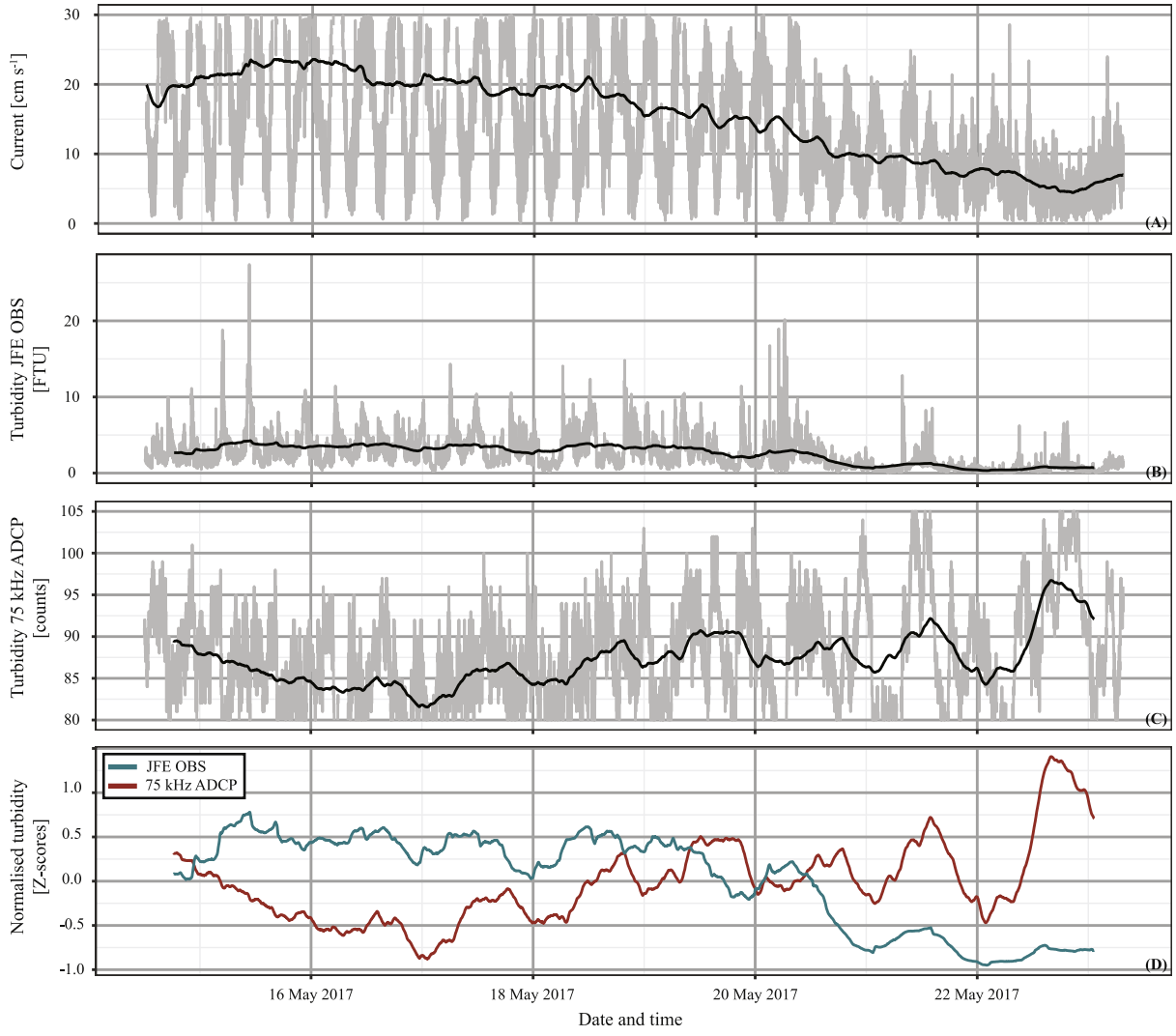

Fig. 9. Nine-day record of a near-bottom (45 mab for 75 kHz ADCP and 5 mab for JFE OBS) time series from the mooring at 1400 m water depth, showing A) current speed, B) turbidity recorded by the JFE Advantech OBS, C) turbidity recorded by the RDI Workhorse 75 kHz ADCP and D) 12.5 h averaged normalised (Z-scores) turbidity records of the JFE Advantech OBS and the RDI Workhorse 75 kHz ADCP. In panels A-C the grey lines represent the actual data, whereas the black lines represent the 12.5 h averaged values. (For interpretation of the references to colour in this figure legend, the reader is referred to the web version of this article.)

the surface water layer than by SPM present in deeper water (Fig. 3A). If not accounted for, this might lead to over- or underestimation of SPM mass concentration. When considering transmissometer output separately for surface water and for deep water, a good correlation was found with SPM mass concentration (Fig. 3C), allowing for a reliable conversion of transmissometer output to SPM mass concentration. In future studies it could be interesting to assess the possibility of using this difference in sensor response as means to determine the relative amount of phytodetritus in the SPM.

Compared to optical turbidity sensors, acoustic devices have the advantage that they are less sensitive to biofouling and therefore are better suited for long-term deployments (de Stigter et al., 2011). Additionally, acoustic profilers collect backscatter data not only from a single spot, but over a range that may extend to several meters in the case of high-frequency profilers. From the consistent logarithmic relationship found between acoustic backscatter recorded by the 1 MHz ADCP and optical backscatter recorded by the OBS (Fig. 5F and 6A), it can be inferred that in that particular case the acoustic and optical sensors were responding to largely overlapping particle size populations. Under such conditions, a quantitative relationship already established between optical backscatter and weighed SPM mass concentration can relatively easily be transferred to a relationship between acoustic backscatter and SPM mass concentration. It should be noted, however, that the sensitivity of the 1 MHz ADCP would increase with an increase of particle size from 24 to 485 μm (lower detection limit to optimum sensitivity), whereas the OBS should decrease in sensitivity over that same particle range. It thus seems preferable, when possible, to calibrate acoustic backscatter directly to SPM from simultaneously collected water samples.

The advantage that high-frequency ADCPs have over optical turbidity sensors, yielding profiles of relative turbidity rather than point measurements, may not apply similarly to low-frequency ADCPs. When operated in downward facing mode to cover the water column up to several hundred of metres above the seafloor, typically the lowermost 25 m above the seafloor, and more in steep terrain, yield unreliable data due to acoustic sidelobe reflections from the seafloor interfering with the signal. However, this could be largely overcome by the usage of ADCPs with a fifth beam, which allows to measure the acoustic backscatter closer to the bottom without interference problems (Wanis, 2013). But even in those ADCPs, data from bins close to the bottom are often compromised by over-reflection. Obviously, for studies of SPM transport in bottom nepheloid layers, the lower tens to hundreds of metres of water column above the seafloor are the most relevant. An even more important disadvantage, is that the low-frequency ADCPs are unable to

detect dispersed fine-grained SPM, which makes up an important part of the total SPM load. By comparing acoustic backscatter recorded by the 75 kHz ADCP with optical backscatter recorded by the OBS (Fig. 6B and 7), it is obvious from the lack of a consistent relationship that these sensors respond to very different particle size population. The 75 kHz ADCP records acoustic backscatter from millimetre-sized particles, which may be flocs of aggregated SPM but could also be zooplankton/nekton, or a combination of both, whereas the optical sensors are most sensitive for the dispersed fine-grained SPM particles in the μm size range. For studies focused on quantification of SPM transport, the preferred choice of sensor therefore seems to be optical sensors like OBSs and transmissometers or high-frequency acoustics sensors, as these usually produce output that is consistent with SPM mass concentrations determined by filtration of water samples.

In places where it may be suspected, or where it is known from in-situ video footage or net hauls, that acoustic backscatter of the 75 kHz ADCP is for an important part associated to the presence of zooplankton/nekton, this type of sensor is obviously unsuited for use in sediment transport studies. But what if material recorded by our 75 kHz ADCP at the bottom of the canyon would indeed be composed for a large part of flocs of aggregated SPM, increasing and decreasing in acoustic records by aggregation and disaggregation under influence of variable current shear? Then the 75 kHz ADCP would convey information about SPM dynamics complementary to what is recorded by the optical and high-frequency acoustic sensors. If that the conspicuous peaks in optical backscatter shown in Fig. 7 were indeed produced by disaggregation of larger aggregates, then from the values presented in this figure we may derive a crude idea of the distribution of SPM over fine-grained dispersed versus aggregated SPM. On top of fluctuating base levels of turbidity of 2–5 FTU, sharp excursions of 10, 15 and up to 25 FTU occurred. This would suggest that these larger aggregates contained the same or up to four times the amount of SPM mass as the background of fine-grained dispersed SPM. This is a substantial amount that should not be overlooked in the quantification of SPM. Quantification of the low-frequency ADCP's backscatter signal in terms of SPM mass concentration remains challenging, however, due to the dependency of the signal on both concentration and particle size.

Independent information on SPM particle size distribution would help to reduce uncertainties. For example by the use of a Laser In-Situ Scattering and Transmission (LISST) sensor for particle size up to 500 μm (Sequoia Inc.; Agrawal and Pottsmith, 2000), and a particle camera for larger particles and aggregates (e.g. Sternberg et al., 1996; Mikkelsen et al., 2005; Davies et al., 2012; Roberts et al., 2018). Whereas particle size distributions of collected water samples measured ex-situ, as illustrated in Fig. 4, only represent the size distribution of primary particles in disaggregated SPM, the LISST sensor and particle camera have the advantage that they give insight in the in-situ particle size distribution of SPM. Multi-frequency acoustic devices such as AQUAscat (Aquatec; Hunter et al., 2012) also hold promise for a more comprehensive quantification of SPM, covering a broader range of particles. Presently, however, these sensors have a maximum particle detection limit of 500 μm, and with a depth rating of 1000 m the application of this device is limited to shelf and upper slope depths. Furthermore, the use of particle cameras in combination with turbidity sensors is important for determining the nature of backscattering particles, whether it is zooplankton/nekton or non-living aggregated particulate matter.

Strong variation in particle size distribution of suspended matter, such as we infer from our observations from Whittard Canyon, is a common feature in dynamic marine systems (e.g. Thomsen and van Weering, 1998; Thomsen et al., 2002; de Stigter et al., 2007, 2011; Baeye and Fettweis, 2015), which are subjected to seasonal variation due to variable production of organic matter that favours SPM aggregation. (Fettweis and Lee, 2017). In such dynamic systems the use of multiple sensors covering a wide range of SPM particle sizes has the advantage of providing insight in SPM dynamics, even though full quantification of the SPM mass concentration across the full particle size spectrum remains difficult. Insight in SPM dynamics is relevant for understanding and quantifying natural processes of SPM dispersion such as in bottom nepheloid layers and hydrothermal plumes. If the SPM mass concentration can be quantified in combination with chemical composition analysis of the SPM, improved estimates can be made on e.g. carbon, nutrient and (trace) metal transport in these systems, which have vital implications on biological processes and biogeochemical budgets.

Furthermore, the insight in SPM dynamics is relevant for studying SPM dispersion in plumes produced by bottom trawling, dredging and future deep-sea mining operations. As demonstrated by Gillard et al. (2019) for the case of deep-sea mining in the Clarion-Clipperton Zone, flocculation of fine-grained sediment particles into large, fast-sinking aggregates, is likely a major factor determining dispersion of sediment plumes stirred up by mining. Monitoring set-ups should therefore be able to record both the dispersed fine-grained SPM and large aggregates and not overlook one or the other, as both may be important pathways of lateral transport (Gardner et al., 2018b).

6. Conclusion

We have shown that interpretation and quantification of the responses of different types of turbidity sensors is not straightforward, and that SPM mass concentrations are easily over- or underestimated, potentially leading to misinterpretation of the SPM dynamics with implications on our understanding of ocean systems. In this case study in the Whittard Canyon we have found that:

- The transmissometer has a stronger response to material in the biologically productive surface layer compared to SPM found in the deeper part of the water column, most likely due to higher absorption of the light signal emitted by the transmissometer by chlorophyll-bearing phytoplankton. If in the conversion of the transmissometer's response to SPM mass concentration this is not corrected for, it will lead to mis-quantification of the SPM mass concentration.
- The OBSs and high-frequency ADCP displayed corresponding backscatter records, whereas the low-frequency ADCP had a remarkably different backscatter record. This is attributed to the different ranges in particle size sensitivity of the different sensors with the OBS and high-frequency ADCP being most sensitive for finer grained material and the low-frequency ADCP for coarser grained material, like aggregates and zooplankton/nekton.
- It has to be considered that changing sensor response may not only reflect changes in SPM mass concentrations, but is also influenced by changing particle size distribution of the SPM. Even though quantification of the low-frequency ADCP's response remains difficult, the combination of this sensor with an OBS, as on our mooring, can potentially provide qualitative information about the aggregation state of the SPM. This allows studying recurring cycles of resuspension involving aggregation and disaggregation of SPM under different turbulence intensities.
- If it can be verified that the acoustic backscatter recorded by the low-frequency ADCP partially represents aggregated SPM, than it should be considered that these aggregates may contain a substantial portion of total SPM, which may remain undetected by using optical and high-frequency acoustic sensors only.
- If it can be verified that the low-frequency ADCP's acoustic backscatter response reflects the presence of zooplankton/nekton, the recorded signal is obviously of no use for sediment transport studies, but it would contain relevant biological information on distribution of zooplankton and nekton. With the caveat again that backscatter intensity is not only determined by biomass but also by size distribution of the zooplankton/nekton.

In general, also when applied to other settings than submarine

canyons, we recommend combining optical and acoustic devices to obtain records on turbidity and current speed and direction in combination with water sampling to determine SPM mass concentration. Furthermore, it is important to determine what type of material is detected by the different type of sensors in order to determine to which degree the recorded turbidity by a sensor can actually be used in sediment transport studies.

Data availability

CTD, lander and mooring data presented in this work, as well as filter weights for SPM sampling and data on particle size analysis of the SPM and surface sediments are available in PANGAEA (https://doi.pangaea.de/10.1594/PANGAEA.927919) and the NIOZ data portal (http://dataverse.nioz.nl/dataverse/doi under DOI 10.25850/nioz/7b.b.hb).

Declaration of Competing Interest

The authors declare that they have no conflict of interest.

Acknowledgements

We thank the captain and crew of RV *Pelagia*, as well as the NIOZ technicians, for their essential assistance during cruises 64PE421 and 64PE437. Jonathan Kranenburg performed the particle size distribution analysis of the surface sediment samples. This research has been supported by the Innovational Research Incentives Scheme of the Netherlands Organisation for Scientific Research (NWO-VIDI grant no. 0.16.161.360) and ship time was provided by the Royal Netherlands Institute for Sea Research. Sabine Haalboom received funding from the Blue Nodules project (EC grant agreement no. 688785). Two anonymous reviewers provided constructive criticism which helped to improve the paper.

Appendix A. Supplementary data

Supplementary data to this article can be found online at https://doi.org/10.1016/j.margeo.2021.106439.

References

Agrawal, Y.C., Pottsmith, H.C., 2000. Instruments for particle size and settling velocity observations in sediment transport. Mar. Geol. 168, 89–114. https://doi.org/10.1016/S0025-3227(00)00044-X.

Amaro, T., de Stigter, H., Lavaleye, M., Duineveld, G., 2015. Organic matter enrichment in the Whittard Channel; its origin and possible effects on benthic megafauna. Deep-Sea Res. Part I – Oceanogr. Res. Papers 102, 90–100. https://doi.org/10.1016/j.dsr.2015.04.014.

Amaro, T., Huvenne, V.A.I., Allcock, A.L., Aslam, T., Davies, J.S., Danovaro, R., De Stigter, H.C., Duineveld, G.C.A., Gambi, C., Gooday, A.J., Gunton, L.M., Hall, R., Howell, K.L., Ingels, J., Kiriakoulakis, K., Kershaw, C.E., Lavaleye, M.S.S., Robert, K., Stewart, H., Van Rooij, D., White, M., Wilson, A.M., 2016. The Whittard Canyon - a case study of submarine canyon processes. Prog. Oceanogr. 146, 38–57. https://doi.org/10.1016/j.pocean.2016.06.003.

Amin, M., Huthnance, J.M., 1999. The pattern of cross-slope depositional fluxes. Deep-Sea Res. Part I-Oceanogr. Res. Papers 46 (9), 1565–1591. https://doi.org/10.1016/S0967-0637(99)00020-5.

Baeye, M., Fettweis, M., 2015. In situ observations of suspended particulate matter plumes at an offshore wind farm, southern North Sea. Geo-Mar. Lett. 35 (4), 247–255. https://doi.org/10.1007/s00367-015-0404-8.

Baker, E.T., Lavelle, J.W., 1984. The effect of particle size on the light attenuation coefficient of natural suspensions. J. Geophys. Res. 89 (C5) https://doi.org/10.1029/JC089iC05p08197.

Bishop, J.K.B., 1986. The correction and suspended particulate matter calibration of sea tech transmissometer data. Deep-Sea Res. Part A-Oceanogr. Res. Papers 33 (1), 121–134. https://doi.org/10.1016/0198-0149(86)90111-1.

Boschen, R.E., Rowden, A.A., Clark, M.R., Gardner, J.P.A., 2013. Mining of deep-sea seafloor massive sulfides: a review of the deposits, their benthic communities, impacts from mining, regulatory frameworks and management strategies. Ocean Coastal Manage 84, 54–67. https://doi.org/10.1016/j.ocecoaman.2013.07.005.

Boss, E., Guidi, L., Richardson, M.J., Stemmann, L., Gardner, W., Bishop, J.K.B., Anderson, R.F., Sherrell, R.M., 2015. Optical techniques for remote and in-situ characterization of particles pertinent to GEOTRACES. Prog. Oceanogr. 133, 43–54. https://doi.org/10.1016/j.pocean.2014.09.007.

Bricaud, A., Morel, A., Babin, M., Allali, K., Claustre, H., 1998. Variations of light absorption by suspended particles with chlorophyll a concentration in oceanic (case 1) waters: Analysis and implications for bio-optical models. J. Geophys. Res. Oceans 103 (C13), 31033–31044. https://doi.org/10.1029/98JC02712.

Briseño-Avena, C., Franks, P.J.S., Roberts, P.L.D., Jaffe, J.S., 2018. A diverse group of echogenic particles observed with a broadband, high frequency echosounder. J. Mar. Sci. 75, 471–482. https://doi.org/10.1093/icesjms/fsx171.

Bunt, J.A.C., Larcombe, P., Jago, C.F., 1999. Quantifying the response of optical backscatter devices and transmissometers to variations in suspended particulate matter. Cont. Shelf Res. 19 (9), 1199–1220. https://doi.org/10.1016/S0278-4343(99)00018-7.

Burd, B.J., Thomson, R.E., 2019. Seasonal patterns in deep acoustic backscatter layers near vent plumes in the northeastern Pacific Ocean. Facets 4, 183–209. https://doi.org/10.1139/facets-2018-0027.

Canals, M., Company, J.B., Martín, D., Sànchez-Vidal, A., Ramírez-Llodrà, E., 2013. Integrated study of Mediterranean deep canyons. Novel results and future challenges. Prog. Oceanogr 118, 1–27. https://doi.org/10.1016/j.pocean.2013.09.004.

Daly, E., Johnson, M.P., Wilson, A.M., Gerritsen, H.D., Kiriakoulakis, K., Allcock, A.L., White, M., 2018. Bottom trawling at Whittard Canyon: evidence for seabed modification, trawl plumes and food source heterogeneity. Prog. Oceanogr. 169, 227–240. https://doi.org/10.1016/j.pocean.2017.12.010.

Davies, E.J., Nimmo-Smith, W.A.M., Agrawal, Y.C., Souza, A.J., 2012. LISST-100 response to large particles. Mar. Geol. 307-310, 117–122. https://doi.org/10.1016/j.margeo.2012.03.006.

Davison, J.J., van Haren, H., Hosegood, P., Piechaud, N., Howell, K.L., 2019. The distribution of deep-sea sponge aggregations (Porifera) in relation to oceanographic processes in the Faroe-Shetland Channel. Deep Sea Res. Part I: Oceanogr. Res. Papers 146, 55–61. https://doi.org/10.1016/j.dsr.2019.03.005.

De Leo, F.C., Smith, C.R., Rowden, A.A., Bowden, D.A., Clark, M.R., 2010. Submarine canyons: hotspots of benthic biomass and productivity in the deep sea. Proc. Biol. Sci. 277 (1695), 2783–2792. https://doi.org/10.1098/rspb.2010.0462.

De Leo, F.C., Ogata, B., Sastri, A.R., Heesemann, M., Mihály, S., Galbraith, M., Morley, M.G., 2018. High-frequency observations from a deep-sea cabled observatory reveal seasonal overwintering of *Neocalanus* ssp. in Barkley Canyon, NE Pacific: Insights into particulate organic carbon flux. Prog. Oceanogr. 169, 120–137. https://doi.org/10.1016/j.pocean.2018.06.001.

de Stigter, H.C., Boer, W., de Jesus Mendes, P.A., Jesus, C.C., Thomsen, L., van den Bergh, G.D., van Weering, T.C.E., 2007. Recent sediment transport and deposition in the Nazaré Canyon, Portuguese continental margin. Mar. Geol. 246 (2–4), 144–164. https://doi.org/10.1016/j.margeo.2007.04.011.

de Stigter, H.C., Jesus, C.C., Boer, W., Richter, T.O., Costa, A., van Weering, T.C.E., 2011. Recent sediment transport and deposition in the Lisbon–Setúbal and Cascais submarine canyons, Portuguese continental margin. Deep-Sea Res. II Top. Stud. Oceanogr. 58 (23–24), 2321–2344. https://doi.org/10.1016/j.dsr2.2011.04.001.

Dickson, R.R., Mccave, I.N., 1986. Nepheloid layers on the continental-slope west of Porcupine Bank. Deep-Sea Res. Part A-Oceanogr. Res. Papers 33 (6), 791–818. https://doi.org/10.1016/0198-0149(86)90089-0.

Downing, J., 2006. Twenty-five years with OBS sensors: the good, the bad, and the ugly. Cont. Shelf Res. 26 (17–18), 2299–2318. https://doi.org/10.1016/j.csr.2006.07.018.

Downing, J.P., Beach, R.A., 1989. Laboratory apparatus for calibrating optical suspended-solids sensors. Mar. Geol. 86 (2–3), 243–249. https://doi.org/10.1016/0025-3227(89)90053-4.

Duineveld, G.C.A., Lavaleye, M.S.S., Berghuis, E.M., de Wilde, P., 2001. Activity and composition of the benthic fauna in the Whittard Canyon and the adjacent slope. Oceanol. Acta 24 (1), 69–83. https://doi.org/10.1016/S0399-1784(00)01129-4.

Durrieu de Madron, X., 1994. Hydrography and nepheloid structures in the Grand-Rhone canyon. Cont. Shelf Res. 14 (5), 457–477. https://doi.org/10.1016/0278-4343(94)90098-1.

Epping, E., van der Zee, C., Soetaert, K., Helder, W., 2002. On the oxidation and burial of organic carbon in sediments of the Iberian margin and Nazaré Canyon. Prog. Oceanogr 52, 399–431. https://doi.org/10.1016/S0079-6611(02)00017-4.

Fettweis, M., Lee, B., 2017. Spatial and seasonal variation of biomineral suspended particulate matter properties in high-turbid nearshore and low-turbid offshore zones. Water 9 (9). https://doi.org/10.3390/w9090694.

Fettweis, M., Francken, F., Pison, V., Van den Eynde, D., 2006. Suspended particulate matter dynamics and aggregate sizes in a high turbidity area. Mar. Geol. 235 (1–4), 63–74. https://doi.org/10.1016/j.margeo.2006.10.005.

Fettweis, M., Riethmüller, R., Verney, R., Becker, M., Backers, J., Baeye, M., Chapalain, M., Claeys, S., Claus, J., Cox, T., Deloffre, J., Depreiter, D., Druine, F., Flöser, G., Grünler, S., Jourdin, F., Lafite, R., Nauw, J., Nechad, B., Röttgers, R., Sottolichio, A., Van Engeland, T., Vanhaverbeke, W., Vereecken, H., 2019. Uncertainties associated with in situ high-frequency long-term observations of suspended particulate matter concentration using optical and acoustic sensors. Prog. Oceanogr. 178 https://doi.org/10.1016/j.pocean.2019.102162 article 102162.

Fielding, S., Griffiths, G., Roe, H.S.J., 2004. The biological validation of ADCP acoustic backscatter through direct comparison with net samples and model predictions based on acoustic-scattering models. J. Mar. Sci. 61, 184–200. https://doi.org/10.1016/j.icesjms.2003.10.011.

Flagg, C.N., Smith, S.L., 1989. On the use of the acoustic Doppler current profiler to measure zooplankton abundance. Deep Sea Res. Part A 36, 455–474. https://doi.org/10.1016/0198-0149(89)90047-2.

Foote, K.G., 2001. Acoustic scattering by marine organisms. In: Encyclopedia of Ocean Sciences, 1. Academic Press, London, pp. 44–53.
Fugate, D.C., Friedrichs, C.T., 2002. Determining concentration and fall velocity of estuarine particle populations using ADV, OBS and LISST. Cont. Shelf Res. 22 (11–13), 1867–1886. https://doi.org/10.1016/S0278-4343(02)00043-2.
García, R., Thomsen, L., 2008. Bioavailable organic matter in surface sediments of the Nazaré canyon and adjacent slope (Western Iberian Margin). J. Mar. Syst. 74 (1–2), 44–59. https://doi.org/10.1016/j.jmarsys.2007.11.004.
Gardner, W.D., 1989. Baltimore Canyon as a Modern Conduit of Sediment to the Deep-Sea. Deep-Sea Res. Part A-Oceanogr. Res. Papers 36 (3), 323–358. https://doi.org/10.1016/0198-0149(89)90041-1.
Gardner, W.D., Richardson, M.J., Mishonov, A.V., Biscaye, P.E., 2018a. Global comparison of benthic nepheloid layers based on 52 years of nephelometer and transmissometer measurements. Prog. Oceanogr. 168, 100–111. https://doi.org/10.1016/j.pocean.2018.09.008.
Gardner, W.D., Richardson, M.J., Mishonov, A.V., 2018b. Global assessment of benthic nepheloid layers and linkage with upper ocean dynamics. Earth Planet. Sci. Lett. 482, 126–134. https://doi.org/10.1016/j.epsl.2017.11.008.
German, C.R., Richards, K.J., Rudnicki, M.D., Lam, M.M., Charlou, J.L., Party, F.S., 1998. Topographic control of a dispersing hydrothermal plume. Earth Planet. Sci. Lett. 156 (3–4), 267–273. https://doi.org/10.1016/S0012-821X(98)00020-X.
Gibbs, R.J., 1978. Light-scattering from particles of different shapes. J. Geophys. Res. Oceans Atmosph. 83 (Nc1), 501–502. https://doi.org/10.1029/JC083iC01p00501.
Gibbs, R.J., Wolanski, E., 1992. The effect of flocs on optical backscattering measurements of suspended material concentration. Mar. Geol. 107 (4), 289–291. https://doi.org/10.1016/0025-3227(92)90078-V.
Gillard, B., Purkiani, K., Chatzievangelou, D., Vink, A., Iversen, M.H., Thomsen, L., 2019. Physical and hydrodynamic properties of deep sea mining-generated, abyssal sediment plumes in the Clarion Clipperton Fracture Zone (eastern-central Pacific). Elementa – Sci. Anthropocene 7. https://doi.org/10.1525/elementa.343.
Glover, A.G., Smith, C.R., 2003. The deep-sea floor ecosystem: current status and prospects of anthropogenic change by the year 2025. Environ. Conserv. 30 (3), 219–241. https://doi.org/10.1017/S0376892903000225.
Gostiaux, L., van Haren, H., 2010. Extracting meaningful information from uncalibrated backscattered echo intensity data. J. Atmos. Ocean. Technol. 27 (5), 943–949. https://doi.org/10.1175/2009JTECHO704.1.
Gruber, P., Felix, D., Storti, G., Lattuada, M., Fleckenstein, P., Deschwanden, F., 2016. Acoustic measuring techniques for suspended sediment. In: IOP Conference Series: Earth and Environmental Science, p. 49.
Guerrero, M., Szupiany, R.N., Amsler, M., 2011. Comparison of acoustic backscattering techniques for suspended sediments investigation. Flow Meas. Instrum. 22 (5), 392–401. https://doi.org/10.1016/j.flowmeasinst.2011.06.003.
Guillén, J., Palanques, A., Puig, P., De Madron, X.D., Nyffeler, F., 2000. Field calibration of optical sensors for measuring suspended sediment concentration in the western Mediterranean. Sci. Mar. 64 (4), 427–435. https://doi.org/10.3989/scimar.2000.64n4427.
Haalboom, S., Price, D.M., Mienis, F., van Bleijswijk, J.D.L., de Stigter, H.C., Witte, H.J., Reichart, G.-J., Duineveld, G.C.A., 2020. Patterns of (trace) metals and microorganisms in the Rainbow hydrothermal vent plume at the Mid-Atlantic Ridge. Biogeosciences 17 (9), 2499–2519. https://doi.org/10.5194/bg-17-2499-2020.
Hall, R.A., Aslam, T., Huvenne, V.A.I., 2017. Partly standing internal tides in a dendritic submarine canyon observed by an ocean glider. Deep Sea Res. Part I: Oceanogr. Res. Papers 126, 73–84. https://doi.org/10.1016/j.dsr.2017.05.015.
Harris, P.T., Whiteway, T., 2011. Global distribution of large submarine canyons: Geomorphic differences between active and passive continental margins. Mar. Geol. 285 (1–4), 69–86. https://doi.org/10.1016/j.margeo.2011.05.008.
Hatcher, A., Hill, P., Grant, J., Macpherson, P., 2000. Spectral optical backscatter of sand in suspension: effects of particle size, composition and colour. Mar. Geol. 168 (1–4), 115–128. https://doi.org/10.1016/S0025-3227(00)00042-6.
Hatcher, A., Hill, P., Grant, J., 2001. Optical backscatter of marine flocs. J. Sea Res. 46 (1), 1–12. https://doi.org/10.1016/S1385-1101(01)00066-1.
Hawley, N., 2004. A comparison of suspended sediment concentrations measured by acoustic and optical sensors. J. Great Lakes Res. 30 (2), 301–309. https://doi.org/10.1016/S0380-1330(04)70348-2.
Hill, P.S., Boss, E., Newgard, J.P., Law, B.A., Milligan, T.G., 2011. Observations of the sensitivity of beam attenuation to particle size in a coastal bottom boundary layer. J. Geophys. Res. 116 (C2) https://doi.org/10.1029/2010JC006539.
Holt, J.T., Thorpe, S.A., 1997. Propagation of high frequency internal waves in the Celtic Sea. Deep-Sea Res. I 44 (12), 2087–2116. https://doi.org/10.1016/S0967-0637(97)00091-5.
Hosegood, P., Bonnin, J., van Haren, H., 2004. Solibore-induced sediment resuspension in the Faeroe-Shetland Channel. Geophys. Res. Lett. 31, L09301 https://doi.org/10.1029/2004GL019544.
Hunter, T.N., Darlison, L., Peakall, J., Biggs, S., 2012. Using a multi-frequency acoustic backscatter system as an in situ high concentration dispersion monitor. Chem. Eng. Sci 80, 409–418. https://doi.org/10.1016/j.ces.2012.06.038.
Huvenne, V.A., Tyler, P.A., Masson, D.G., Fisher, E.H., Hauton, C., Huhnerbach, V., Le Bas, T.P., Wolff, G.A., 2011. A picture on the wall: innovative mapping reveals cold-water coral refuge in submarine canyon. PLoS One 6 (12), e28755. https://doi.org/10.1371/journal.pone.0028755.
Ibáñez-Tejero, L., Ladah, L.B., Sánchez-Velasco, L., Barton, E.D., Filonov, A., 2018. Vertical distribution of zooplankton biomass during internal tidal forcing under mesoscale conditions of upwelling and relaxation. Continental Shelf Res 171, 1–11. https://doi.org/10.1016/j.csr.2018.10.003.
Jahnke, R.A., Reimers, C.E., Craven, D.B., 1990. Intensification of recycling of organic-matter at the sea-floor near ocean margins. Nature 348 (6296), 50–54. https://doi.org/10.1038/348050a0.
Jerlov, N.G., 1976. Marine Optics, Chapter 3. Elsevier, New York.
Khripounoff, A., Vangriesheim, A., Crassous, P., Segonzac, M., Colaço, A., Desbruyères, D., Barthelemy, R., 2001. Particle flux in the Rainbow hydrothermal vent field (Mid-Atlantic Ridge), Dynamics, mineral and biological composition. J. Mar. Res. 59 (4), 633–656. https://doi.org/10.1357/002224001762842217.
Kineke, G.C., Sternberg, R.W., 1992. Measurements of high concentration suspended sediment using the optical backscatterance sensor. Mar. Geol 108, 253–258. https://doi.org/10.1016/0025-3227(92)90199-R.
Kiriakoulakis, K., Blackbird, S., Ingels, J., Vanreusel, A., Wolff, G.A., 2011. Organic geochemistry of submarine canyons: the Portuguese Margin. Deep-Sea Res. II Top. Stud. Oceanogr. 58 (23–24), 2477–2488. https://doi.org/10.1016/j.dsr2.2011.04.010.
Kutti, T., Bannister, R.J., Fosså, J.H., Krogness, C.M., Tjensvoll, I., Søvik, G., 2015. Metabolic responses of the deep-water sponge Geodia barretti to suspended bottom sediment, simulated mine tailings and drill cuttings. J. Exp. Mar. Biol. Ecol. 473, 64–72. https://doi.org/10.1016/j.jembe.2015.07.017.
Lewis, J., Eads, R., Klein, R., 2007. Comparisons of Turbidity Data Collected with Different Instruments. California Department of Forestry and Fire Protection USDA Forest Service - Pacific Southwest Research Station.
Lin, J., He, Q., Guo, L., van Prooijen, B.C., Wang, Z.B., 2020. An integrated optic and acoustic (IOA) approach for measuring suspended sediment concentration in highly turbid environments. Mar. Geol. 421 https://doi.org/10.1016/j.margeo.2019.106062 article number 106062.
Lohrmann, A., 2001. Monitoring Sediment Concentration with Acoustic Backscattering Instruments. Nortek.
Maa, J.P.Y., Xu, J.P., Victor, M., 1992. Notes on the performance of an optical backscatter sensor for cohesive sediments. Mar. Geol. 104 (1–4), 215–218. https://doi.org/10.1016/0025-3227(92)90096-Z.
Manning, A.J., Dyer, K.R., 1999. A laboratory examination of floc characteristics with regard to turbulent shearing. Mar. Geol. 160, 147–170. https://doi.org/10.1016/S0025-3227(99)00013-4.
Markussen, T.N., Andersen, T.J., 2014. Flocculation and floc break-up related to tidally induced turbulent shear in a low-turbidity, microtidal estuary. J. Sea Res. 89, 1–11. https://doi.org/10.1016/j.seares.2014.02.001.
Martín, J., Puig, P., Palanques, A., Giamportone, A., 2014. Commercial bottom trawling as a driver of sediment dynamics and deep seascape evolution in the Anthropocene. Anthropocene 7, 1–15. https://doi.org/10.1016/j.ancene.2015.01.002.
McAnally, W.H., Mehta, A.J., 2002. Significance of aggregation of fine sediment particles in their deposition. Estuar. Coastal Shelf Sci. 54, 643–653. https://doi.org/10.1006/ecss.2001.0847.
McCave, I.N., 1986. Local and global aspects of the bottom nepheloid layers in the world ocean. Neth. J. Sea Res. 20 (2/3), 167–181. https://doi.org/10.1016/0077-7579(86)90040-2.
Merckelbach, L.M., Ridderinkhof, H., 2005. Estimating suspended sediment concentration using backscatterance from an acoustic Doppler profiling current meter at a site with strong tidal currents. Ocean Dyn. 56 (3–4), 153–168. https://doi.org/10.1007/s10236-005-0036-z.
Mienis, F., de Stigter, H.C., White, M., Duineveld, G., de Haas, H., van Weering, T.C.E., 2007. Hydrodynamic controls on cold-water coral growth and carbonate-mound development at the SW and SE Rockall Trough Margin, NE Atlantic Ocean. Deep-Sea Res. I Oceanogr. Res. Pap. 54 (9), 1655–1674. https://doi.org/10.1016/j.dsr.2007.05.013.
Mikkelsen, O.A., Hill, P.S., Milligan, T.G., Chant, R.J., 2005. In situ particle size distributions and volume concentrations from a LISST-100 laser particle sizer and a digital floc camera. Cont. Shelf Res. 25 (16), 1959–1978. https://doi.org/10.1016/j.csr.2005.07.001.
Moate, B.D., Thorne, P.D., 2012. Interpreting acoustic backscatter from suspended sediments of different and mixed mineralogical composition. Continental Shelf Res 46, 67–82. https://doi.org/10.1016/j.csr.2011.10.007.
Mullison, J., 2017. Backscatter Estimation Using Broadband Acoustic Doppler Current Profilers Application Note (FSA-031), Teledyne RD Instruments. In: ASCE Hydraulic Measurements and Experimental Methods Conference, Durham, NH.
Ohnemus, D.C., Lam, P.J., Twining, B.S., 2018. Optical observation of particles and responses to particle composition in the GEOTRACES GP16 section. Mar. Chem. 201, 124–136. https://doi.org/10.1016/j.marchem.2017.09.004.
Osborne, P.D., Vincent, C.E., Greenwood, B., 1994. Measurement of suspended sand concentrations in the nearshore - field intercomparison of optical and acoustic backscatter sensors. Cont. Shelf Res. 14 (2–3), 159–174. https://doi.org/10.1016/0278-4343(94)90011-6.
Perkey, D., Pratt, T., Ganesh, N., 2010. Comparison of SSC measurements with acoustic backscatter data: West Bay sediment diversion, Mississippi River. In: 2nd Joint Federal Interagency Conference: Las Vegas.
Pingree, 1980. Physical Oceanography of the Celtic Sea and English Channel. In: Elsevier Oceanography Series, volume 24, part B, pp. 415–465. https://doi.org/10.1016/S0422-9894(08)71358-8.
Plueddemann, A.J., Pinkel, P., 1989. Characterization of the patterns of diel migration using a Doppler sonar. Deep Sea Res., Part A 36, 509–530. https://doi.org/10.1016/0198-0149(89)90003-4.
Puig, P., Palanques, A., 1998. Nepheloid structure and hydrographic control on the Barcelona continental margin, northwestern Mediterranean. Mar. Geol. 149 (1–4), 39–54. https://doi.org/10.1016/S0025-3227(98)00037-1.

Puig, P., Canals, M., Company, J.B., Martin, J., Amblas, D., Lastras, G., Palanques, A., 2012. Ploughing the deep sea floor. Nature 489 (7415), 286–289. https://doi.org/10.1038/nature11410.

Puig, P., Palanques, A., Martin, J., 2014. Contemporary sediment-transport processes in submarine canyons. Ann. Rev. Mar. Sci. 6, 53–77. https://doi.org/10.1146/annurev-marine-010213-135037.

Quaresma, L.S., Vitorino, J., Oliveira, A., da Silva, J., 2007. Evidence of sediment resuspension by nonlinear internal waves on the western Portuguese mid-shelf. Mar. Geol. 246 (2–4), 123–143. https://doi.org/10.1016/j.margeo.2007.04.019.

R Core Team, 2020. R: A Language and Environment for Statistical Computing. R Foundation for Statistical Computing, Vienna, Austria. https://www.R-project.org/.

Roberts, E.M., Mienis, F., Rapp, H.T., Hanz, U., Meyer, H.K., Davies, A.J., 2018. Oceanographic setting and short-timescale environmental variability at an Arctic seamount sponge ground. Deep Sea Res. Part I: Oceanogr. Res. Papers 138, 98–113. https://doi.org/10.1016/j.dsr.2018.06.007.

Robertson, C.M., Demopoulos, A.W.J., Bourque, J.R., Mienis, F., Duineveld, G.C.A., Lavaleye, M.S.S., Koivisto, R.K.K., Brooke, S.D., Ross, S.W., Rhode, M., Davies, A.J., 2020. Submarine canyons influence macrofaunal diversity and density patterns in the deep-sea benthos. Deep Sea Res. Part I, Oceanogr. Res. Papers 159. https://doi.org/10.1016/j.dsr.2020.103249 volume.

Rymszewicz, A., O'Sullivan, J.J., Bruen, M., Turner, J.N., Lawler, D.M., Conroy, E., Kelly-Quinn, M., 2017. Measurement differences between turbidity instruments, and their implications for suspended sediment concentration and load calculations, A sensor inter-comparison study. J. Environ. Manage 199, 99–108. https://doi.org/10.1016/j.jenvman.2017.05.017.

Sahin, C., Ozturk, M., Aydogan, B., 2020. Acoustic doppler velocimeter backscatter for suspended sediment measurements: Effects of sediment size and attenuation. Appl. Ocean Res. 94 https://doi.org/10.1016/j.apor.2019.101975 article 101975.

Santos, A.I., Oliveira, A., Carinhas, D., Pinto, J.P., Zacarias, N., Freitas, M.C., 2020. The acoustic properties of in-situ measured suspended sediments and their implications on concurrent ADCP response – Case studies of the Portuguese inner shelf. Mar. Geol. 419 https://doi.org/10.1016/j.margeo.2019.106079 article 106079.

Schaafsma, A.S., Hay, A.E., 1997. Attenuation in suspensions of irregularly shaped sediment particles: a two-parameter equivalent spherical scatterer model. J. Acoustical Soc. Am. 102 (3), 1485–1502. https://doi.org/10.1121/1.420063.

Schoellhamer, D.H., 1993. Biological interference of optical backscatterance sensors in Tampa Bay, Florida. Mar. Geol. 110, 303–313. https://doi.org/10.1016/0025-3227(93)90090-I.

Smith, S.J., Friedrichs, C.T., 2011. Size and settling velocities of cohesive flocs and suspended sediment aggregates in a trailing suction hopper dredge plume. Cont. Shelf Res. 31 (10), S50–S63. https://doi.org/10.1016/j.csr.2010.04.002.

Sternberg, R.W., Ogston, A., Johnson, R., 1996. A video system for in situ measurement of size and settling velocity of suspended particles. J. Sea Res. 36, 127–130. https://doi.org/10.1016/S1385-1101(96)90782-0.

Thomsen, L., 1999. Processes in the benthic boundary layer at continental margins and their implications for the benthic carbon cycle. J. Sea Res. 41, 73–86. https://doi.org/10.1016/S1385-1101(98)00039-2.

Thomsen, L., Gust, G., 2000. Sediment erosion thresholds and characteristics of resuspended aggregates on the western European continental margin. Deep-Sea Res. Part I 47, 1881–1897. https://doi.org/10.1016/S0967-0637(00)00003-0.

Thomsen, L., van Weering, T.C.E., 1998. Spatial and temporal variability of particulate matter in the benthic boundary layer at the N.W. European Continental Margin (Goban Spur). Prog. Oceanogr. 42, 61–76. https://doi.org/10.1016/S0079-6611(98)00028-7.

Thomsen, L., van Weering, T., Gust, G., 2002. Processes in the benthic boundary layer at the Iberian continental margin and their implication for carbon mineralization. Prog. Oceanogr. 52 (2–4), 315–329. https://doi.org/10.1016/S0079-6611(02)00013-7.

Thorne, P.D., Hanes, D.M., 2002. A review of acoustic measurement of small-scale sediment processes. Cont. Shelf Res. 22 (4), 603–632. https://doi.org/10.1016/S0278-4343(01)00101-7.

van de Hulst, H.C., 1957. Light Scattering by Small Particles. Wiley, New York.

van den Eynde, D., Baeye, M., Fettweis, M., Francken, F., Naudts, L., Van Lancker, V., 2014. Sediment Plume Monitoring in the Clarion-Clipperton Zone, 2nd Deep-Water Circulation Congress, Ghent, Belgium.

van Haren, H., 2007. Monthly periodicity in acoustic reflections and vertical motions in the deep ocean. Geophys. Res. Lett. 34, L12603 https://doi.org/10.1029/2007GL029947.

van Haren, H., Compton, T.J., 2013. Diel vertical migration in deep sea plankton is finely tuned to latitudinal and seasonal day length. PLoS One 8 (5). https://doi.org/10.1371/journal.pone.0064435 article e64435.

van Haren, H., Laan, M., Buijsman, D.-J., Gostiaux, L., Smit, M.G., Keijzer, E., 2009. NIOZ3: Independent temperature sensors sampling year-long data at a rate of 1 Hz. IEEE J. Oceanic Eng 24, 315–322.

van Haren, H., Cimatoribus, A.A., Gostiaux, L., 2015. Where large deep-ocean waves break. Geophys. Res. Lett. 42, 2351–2357. https://doi.org/10.1002/2015GL063329.

van Leussen, W., 1988. Aggregation of particles, settling velocity of mud flocs - a review. In: Dronkers, J., van Leussen, W. (Eds.), Physical Processes in Estuaries. Springer Verlag, pp. 347–403.

Verney, R., Lafite, R., Brun-Cottan, J.C., Le Hir, P., 2011. Behaviour of a floc population during a tidal cycle: laboratory experiments and numerical modelling. Cont. Shelf Res. 31, S64–S83. https://doi.org/10.1016/j.csr.2010.02.005.

Walsh, J.J., 1991. Importance of continental margins in the marine biogeochemical cycling of carbon and nitrogen. Nature 350, 53–55. https://doi.org/10.1038/350053a0.

Wanis, P., 2013. Design and Applications of a Vertical Beam in Acoustic Doppler Current Profilers. OCEANS – San Diego, San Diego, CA, pp. 1–5.

Wilson, G.W., Hay, A.E., 2015. Acoustic backscatter inversion for suspended sediment concentration and size: a new approach using statistical inverse theory. Continental Shelf Res. 106, 130–139. https://doi.org/10.1016/j.csr.2015.07.005.

Wilson, A.M., Raine, R., Mohn, C., White, M., 2015. Nepheloid layer distribution in the Whittard Canyon, NE Atlantic Margin. Mar. Geol. 367, 130–142. https://doi.org/10.1016/j.margeo.2015.06.002.

Yang, C., Xu, D., Chen, Z., Wang, J., Xu, M., Yuan, Y., Zhou, M., 2019. Diel vertical migration of zooplankton and micronekton on the northern slope of the South China Sea observed by a moored ADCP. Deep-Sea Res. Part II 167, 93–104. https://doi.org/10.1016/j.dsr2.2019.04.012 volume.

Ziegler, A.C., 2002. Issues related to use of turbidity measurements as a surrogate for suspended sediment. In: Turbidity and Other Sediment Surrogates Workshop, April 30 – May 2, 2002, Reno, NV.